

1 **The diurnal cycle of cloud profiles over land and ocean between 51°S and 51°N, seen by the**  
2 **CATS spaceborne lidar from the International Space Station**

3

4 Vincent Noel <sup>1</sup>, H  l  ne Chepfer <sup>2</sup>, Marjolaine Chiriaco <sup>3</sup>, John Yorks <sup>4</sup>

5

6 1 - Laboratoire d'A  rologie, CNRS/UPS, Observatoire Midi-Pyr  n  es, 14 avenue Edouard  
7 Belin, Toulouse, France

8 2 - LMD/IPSL, Sorbonne Universit  ,   cole polytechnique,   cole Normale Sup  rieure, PSL  
9 Research University, CNRS, F-91120 Palaiseau, France

10 3 - LATMOS/IPSL, Univ. Versailles Saint-Quentin en Yvelines, France

11 4 - NASA GSFC, Greenbelt, Maryland, USA

12

13 Proposed for publication in:

14 Atmospheric Chemistry and Physics

15

16 22 June 2018

17

18 **Abstract.**

19 We document, for the first time, how detailed vertical profiles of Cloud Fraction change  
20 diurnally between 51°S and 51°N, by taking advantage of 15 months of measurements from  
21 the Cloud and Aerosol Transport System (CATS) lidar on the non-sun-synchronous  
22 International Space Station (ISS).

23 Over the Tropical ocean in summer, we find few high clouds during daytime. At night they  
24 become frequent over a large altitude range (11-16km between 10PM and 4AM). Over the  
25 summer tropical continents, but not over ocean, CATS observations reveal mid-level clouds  
26 (4-8 km Above Sea Level or ASL) persisting all-day long, with a weak diurnal cycle (minimum  
27 at noon). Over the Southern Ocean, diurnal cycles appear for the omnipresent low-level  
28 clouds (minimum between noon and 3PM) and high-altitude clouds (minimum between  
29 8AM and 2PM). Both cycles are time-shifted, with high-altitude clouds following the  
30 changes in low-altitude clouds by several hours. Over all continents at all latitudes during  
31 summer, the low-level clouds develop upwards and reach a maximum occurrence at about  
32 2.5 km ASL in the early afternoon (around 2 pm).

33 Our work also shows that 1) the diurnal cycles of vertical profiles derived from CATS are  
34 consistent with those from ground-based active sensors at local scale, 2) the cloud profiles  
35 derived from CATS measurements at local times of 0130AM and 0130PM are consistent  
36 with those observed from CALIPSO at similar times, 3) the diurnal cycles of low and high  
37 cloud amounts derived from CATS are in general in phase with those derived from  
38 geostationary imagery but less pronounced. Finally, the diurnal variability of cloud profiles  
39 revealed by CATS strongly suggests that CALIPSO measurements at 0130AM and PM  
40 document the daily extremes of the cloud fraction profiles over ocean and are more  
41 representative of daily averages over land, except at altitudes above 10km where they  
42 capture part of the diurnal variability. These findings are applicable to other instruments  
43 with local overpass times similar to CALIPSO's, like all the other A-Train instruments and the  
44 future Earth-CARE mission.

45

46

47	<b>Outline</b>
48	1. Introduction
49	2. Data and methods
50	2.1 Data
51	a. Cloud detections from the CATS spaceborne Lidar
52	b. Cloud detections from ground-based active instruments
53	c. Cloud detections from passive and active spaceborne sensors
54	2.2 Methods
55	a. Building the diurnal cycle of Cloud Fraction profiles from lidar cloud detections
56	b. Building the diurnal cycle of Low and High Clouds Amounts from CATS data
57	3. Results
58	3.1 Diurnal cycle of Cloud Fraction profiles observed at Global scale
59	3.2 Diurnal cycle of Cloud Fraction profiles observed over mid-latitudes and Tropics
60	a. High clouds
61	b. Low clouds
62	c. Seasonal differences
63	3.3 Diurnal cycle of Cloud Fraction profiles above selected continental regions
64	a. Over South of Paris in Europe
65	b. Over the US Southern Great Plains ARM site
66	c. Over the subtropical Eastern North Atlantic ARM site
67	d. Over continents
68	4. Discussion
69	4.1 About the diurnal cycles of the Low and High Cloud Amounts
70	4.2 About the Cloud Fraction profiles observed at fixed local times by space lidars
71	5. Conclusions
72	

73 **1. Introduction**

74 The diurnal cycle of clouds has been documented for decades by ground-based instruments  
75 (e.g. Gray and Jacobson, 1977) and geostationary satellites (e.g. Rossow et al., 1989). Even  
76 though climatologies give priority on how clouds change with seasons and geography, many  
77 studies noted the strong diurnal cycle of boundary layer clouds. During the day, low clouds  
78 form in the morning and expand, following the warming of the surface by incoming solar  
79 radiation (Stubenrauch et al., 2006). Maximum low cloud amount is often reached in the  
80 early afternoon. This sun-driven variation is maximum over continents, where it depends on  
81 orography (Wilson and Barros, 2017; Shang et al., 2018), and in summer. It is more limited  
82 over ocean and during winter (Rozendaal et al., 1995; Soden, 2000). When night falls,  
83 condensation in the boundary layer can create stratiform clouds, which stabilize and expand  
84 through nighttime radiative cooling at cloud top and reach maximal cover in the early  
85 morning (Greenwald and Christopher, 1999; Eastman and Warren, 2014).

86 In the Tropics, the near-surface daily increase in water vapor triggered by solar warming  
87 (Tian et al., 2004) is transmitted to higher altitudes through deep convection (Johnson et al.,  
88 1999). This imposes a diurnal cycle to high clouds, which is delayed by several hours  
89 compared to low clouds (Soden, 2000). Their maximum amount is reached in the evening  
90 (Rossow and Schiffer, 1999; Stubenrauch et al., 2006). At midlatitudes, without deep  
91 convection most of the troposphere is free from surface influence (Wang and Sassen, 2001),  
92 and diurnal changes in the distribution of high-altitude clouds are limited. Changes are  
93 rather driven by the local atmospheric circulation (e.g. Storm-tracks), leading to less  
94 predictable patterns which are more location-dependent.

95 More recently, geostationary imagery documented the diurnal variations in the composition  
96 of cloud cover above Central Africa (Philippon et al., 2016) and cloud top temperatures  
97 (Taylor et al., 2017). In any case, the vertically-integrated nature of passive imagery means it  
98 cannot resolve the vertical variability of clouds and its diurnal cycle, which is key to better  
99 understand the atmospheric heating rate profile (L'Ecuyer et al., 2008). By comparison,  
100 active remote sensing instruments, such as radars and lidars, document the cloud vertical  
101 distribution with great accuracy and vertical resolutions finer than 500m. Long-running  
102 datasets from active instruments operated from ground-based sites have led to useful time  
103 series and statistics about clouds (e.g. Sassen and Benson, 2001; Hogan et al., 2003; Protat

104 et al., 2009; Dong et al., 2010; Hoareau et al., 2013; Zhao et al., 2016). From space, Liu and  
105 Zipser (2008) were able to derive information on the clouds diurnal cycle from the  
106 spaceborne Tropical Rainfall Measuring Mission radar, launched in 1997 (Kummerow et al.,  
107 1998), but the instrument was not designed to detect clouds with accuracy. The CALIPSO  
108 lidar (Cloud-Aerosol Lidar and Infrared Pathfinder Satellite Observations), since its launch  
109 into orbit in 2006 (Winker et al., 2010), has provided transformative vertically-resolved data  
110 on clouds (Stephens et al., 2017; Winker et al., 2017). Cloud detections from CALIPSO have,  
111 among other things, helped pinpoint and improve significant cloud-related weaknesses in  
112 climate models (e.g. Cesana and Chepfer, 2013; Konsta et al., 2016), helped improve  
113 estimates of the surface radiation budget (Kato et al., 2011) and of the heating rate profile  
114 (Haynes et al., 2013; Bouniol et al., 2016). Due to its sun-synchronous polar orbit, CALIPSO  
115 samples the atmosphere at either 1:30AM or 1:30PM local time (LT), like the CloudSat radar  
116 (Stephens and Kummerow, 2007) and all A-Train instruments (L'Ecuyer and Jiang, 2010).  
117 Even though measurements at two times of day can offer insights into the day-night cloud  
118 changes (Sèze et al., 2015; Gupta et al., 2018), they are insufficient to fully document the  
119 diurnal evolution of cloud profiles. This observational blind spot explains why very little is  
120 known so far about how the vertical distribution of clouds changes diurnally in most of the  
121 globe, leading to inconsistencies amongst climate models (Yin and Porporato, 2017).

122 Here we take advantage of measurements from the Cloud Aerosol Transport System (CATS,  
123 McGill et al., 2015) lidar on the International Space Station (ISS), to document the diurnal  
124 evolution of the vertical distribution of clouds in regions of the globe. As the ISS orbits the  
125 Earth many times a day between 51°S and 51°N, CATS measurements cannot track the  
126 evolution of individual clouds over a given location and a given day. Instead, cloud  
127 detections over a given location at variable times of day can be aggregated over seasons, to  
128 create statistics that eventually document the seasonal average diurnal cycle of clouds over  
129 that location. Thus far, the CATS dataset is the only one to contain active vertically-resolved  
130 measurements made from satellite with variable local times of overpass.

131 We first describe how data were selected and processed to derive diurnal cycles of cloud  
132 Cloud Fraction (CF) profiles and Cloud Amounts (CA) from CATS and all other instruments  
133 included for comparison (Sect. 2). Then, using CATS retrievals we document, for the first  
134 time, the diurnal cycle of detailed Cloud Fraction profiles in large regions of the globe in two

135 seasons over ocean and land (Sect. 3.1 and 3.2). In Sect. 3.3 we describe CATS-derived  
136 diurnal cycles of cloud profiles over selected sites and continents with two goals in mind: (i)  
137 to compare them with independent ground-based observations to check the validity of the  
138 CATS retrievals, and (ii) to document the diversity of the continental cloud profile diurnal  
139 cycles over the globe. In Section 4 we discuss implications of our results: We compare the  
140 diurnal cycle of the Low and High cloud covers derived from CATS with ones from  
141 geostationary satellites (Sect. 4.1), and discuss the agreement between CATS Cloud Fraction  
142 profiles derived at the times of CALIPSO overpass with actual CALIPSO retrievals (Sect.  
143 4.2.a). Finally, we consider CATS profiles at overpass times from current and future sun-  
144 synchronous spaceborne lidar missions (Sect. 4.2.b) to understand which part of the diurnal  
145 cloud cycle is sampled by these instruments. We conclude in Sect. 5.

146 **2. Data and Methods**

147

148 **2.1 Data**

149

150 ***a) Cloud detections from the CATS spaceborne lidar***

151 In this study, our primary data consist of clouds detected during June-July-August (JJA) and  
152 December-January-February (DJF) periods using data from the CATS lidar system (Yorks et  
153 al., in preparation). CATS operated from the ISS between February 2015 to late October  
154 2017. Although CATS was originally designed to operate at 3 wavelengths (355, 532 and  
155 1064nm) with variable viewing geometries, beginning in March 2015 technical issues limited  
156 operation to a single 1064nm wavelength and a single viewing mode. The CATS instrument  
157 went on providing single-channel high-quality data (Yorks et al., 2016a) until a fault in the  
158 on-board power and data system ended science operations on October 30, 2017.

159 Being located on the ISS means measurements from CATS are constrained to latitudes  
160 below 51°, giving it access to ~78% of the Earth's surface (Figure 1, top). This prevents our  
161 study from covering polar regions, but leads to densely distributed overpasses at latitudes  
162 above 40°. CATS sampling is particularly good in populated midlatitude regions and above  
163 the Southern Ocean.

164 CATS reports vertical profiles of Attenuated Total Backscatter (ATB) every 350m at 1064nm  
165 with a 60m vertical resolution (Yorks et al., 2016a). In the mode 7.2 in which CATS operates  
166 since February 2015, each profile is created by accumulating backscattered energy from 200  
167 4kHz pulses, 20 times per second. The CATS vertical feature mask algorithms use these  
168 calibrated ATB profiles, averaged to 5 and 60 km, to detect atmospheric layers, discriminate  
169 clouds from aerosols, and determine cloud phase (Yorks et al., 2016b and in preparation).  
170 The CATS layer-detection algorithms are based on a threshold-profile technique similar to  
171 the one used for CALIOP (Vaughan et al., 2009) but, unlike for CALIOP, they rely primarily on  
172 1064nm ATB (Yorks et al., 2016b). CATS cloud-aerosol discrimination algorithm uses a  
173 probability density function technique that is based on the CALIPSO algorithm but relies on  
174 horizontal persistence tests to differentiate low-level clouds and aerosol because  
175 backscatter color ratio, used in the CALIOP algorithms (Liu et al., 2009), is not available in

176 Mode 7.2. For cloud phase, CATS uses layer-integrated 1064 nm depolarization ratio and  
177 mid-layer temperature thresholds based on Hu et al. (2009) and Yorks et al. (2011).  
178 Minimum horizontal average was 5km in nighttime and 60km in daytime, a choice that  
179 brings the same cloud detection sensitivity to both (Yorks et al., 2016a). This has two  
180 consequences: 1) optically thinnest clouds detected during nighttime at 60km horizontal  
181 averaging might be absent from daytime detections (these represent roughly ~5% of  
182 nighttime clouds) and 2) the horizontal extent and cloud amount of fragmented boundary  
183 layer clouds might be overestimated in both daytime and nighttime compared to single-shot  
184 detections (as in Chepfer et al., 2013; Cesana et al., 2016). Cloud top and base heights,  
185 phase, and other properties are reported in the CATS Level 2 Operational (L2O) products  
186 every 5 km along-track. Hereafter we used such cloud properties from CATS L2O data files  
187 v2.01 (Palm et al., 2016), including only layers with a feature type score above 5, to avoid  
188 including wrongly-classified optically thick aerosol layers near deserts.

189 To document the diurnal cycle (Sect. 2.2.a), we used CATS cloud detections from JJA and DJF  
190 seasons between March 2015 and October 2017. CATS cloud data being still novel at the  
191 time of this writing, we document and discuss several of its characteristics in Appendices A  
192 and B, including sampling variability and the sensitivity of cloud detection in presence of  
193 solar pollution. This exploration of CATS data (and the upcoming comparisons with other  
194 instruments) made us confident that its sampling and cloud detections are robust enough to  
195 be used for scientific purposes.

196

#### 197 ***b) Cloud detections from ground-based active instruments***

198 Like with any lidar, the CATS laser beam gets fully attenuated when passing through clouds  
199 with optical depths larger than typically 3 (e.g., Chepfer et al., 2010). This can lead to the  
200 Cloud Fractions being underestimated in the lower troposphere. Meanwhile, horizontal  
201 averaging during daytime can lead to Cloud Fractions being overestimated at low altitudes.  
202 To estimate how much the CATS Cloud Fraction is biased at low altitudes, we compare CATS  
203 detections with independent observations collected from ground-based active instruments.  
204 Ground-based observation sites provide long-term records of atmospheric properties over  
205 periods that often cannot be reached by satellite instruments (Chiriaco et al., 2018).



206 Nowadays such sites are often well equipped with active remote sensing instruments. Data  
207 acquisition, calibration and processing are often homogenized in the framework of specific  
208 observation networks (e.g. EARLINET, the European Aerosol Research Lidar Network,  
209 Pappalardo et al., 2014). Descriptions of the clouds diurnal cycle based on active ground-  
210 based measurements are however scarce. In this study, we compare CATS cloud cycles with  
211 those derived from active measurements at three ground-based sites, two continental and  
212 one oceanic:

- 213 • The Site Instrumenté de Recherche par Télédétection Atmosphérique (SIRTA,  
214 Haeffelin et al., 2005) is continental, located 20km South-West of Paris at 48.7°N,  
215 2.2°E. From SIRTA we used cloud detections from the Lidar Nuages et Aérosols (LNA,  
216 Elouragini and Flamant, 1996), which were curated, packaged and made available in  
217 the framework of the SIRTA-reOBS project (Chiriaco et al., 2014, 2018). The LNA  
218 requires human supervision and does not operate under precipitation, leading to  
219 irregular sampling and almost no nighttime measurements. Thanks to its long  
220 operation time, its cloud dataset covers almost 15 years and was used in many  
221 studies (e.g. Noel and Haeffelin, 2007; Naud et al., 2010; Dupont et al., 2010). Cloud  
222 layers were detected in LNA profiles of attenuated backscatter following a threshold-  
223 based approach similar to CATS and CALIPSO.
- 224 • The Atmospheric Radiation Measurement (ARM) Southern Great Plains (SGP) site is  
225 continental too, at 97°W, 36°N. From ARM-SGP we used the sgparsclkazr1kolliasC1  
226 cloud dataset (DOI: 10.5439/1393437), which contains vertical cloud detection  
227 profiles for every second every day based on measurements from the 35GHz Ka ARM  
228 Zenith Radar. This instrument has been operating since 2011 (Kollias et al., 2014).  
229 Based on these profiles we reconstructed hourly averages of Cloud Fraction profiles  
230 over seasons during the CATS operation period. Our results closely match those Zhao  
231 et al. (2017) derived from the same instrument, and those Dupont (2011) derived  
232 from the ARM-SGP Raman lidar.
- 233 • The ARM Eastern North Atlantic (ENA) site is oceanic, located on Graciosa Island in  
234 the Azores archipelago (28.03°W, 39.1°N). From ARM-ENA we used cloud detections  
235 from the enaarsclkazr1kolliasC1 dataset derived from a 35GHz radar similar to the  
236 one found at SGP, which we processed in a similar way.

237

238 ***c) Cloud detections from passive and active spaceborne sensors***

239 In addition to the datasets from CATS, LNA and two ground-based radars, in the  
240 upcoming sections we use cloud retrievals from two spaceborne datasets to put CATS cloud  
241 retrievals into a referenced context. First, we consider the baseline reference for the  
242 description of the clouds diurnal cycle from space: the analysis of data from the ISCCP done  
243 by Rossow and Schiffer (1999), hereafter RS99. Their results are based on aggregated and  
244 homogenized infrared and visible radiances from imaging radiometers on the international  
245 constellation of weather satellites. They are widely considered as the reference for  
246 describing the diurnal cycle of the cloud cover at large scales from space measurements. We  
247 did not reprocess any ISCCP data for the present study, instead we rely on the description of  
248 the diurnal cycle of low and high clouds RS99 documented in their Fig. 11 based on ISCCP, to  
249 which we confront CATS retrievals in Sect. 4.1.

250 Finally, we also confront CATS cloud detections with retrievals based on measurements  
251 from the CALIOP lidar, routinely made since 2006 from the sun-synchronous CALIPSO  
252 platform at 13:30 and 01:30 LT in Sect. 4.2. To enable comparison with CATS retrievals, we  
253 used cloud layers retrieved from CALIPSO measurements during the period of CATS  
254 operation (March 2015 to October 2017) and documented at a 5km horizontal resolution in  
255 CALIPSO Level 2 V4.10 Cloud Layer Products (Vaughan et al., 2009). We processed both  
256 CATS and CALIPSO data alike as described in Sect. 2.2.a.

257

258 **2.2. Methods**

259

260 ***a) Building the diurnal cycle of Cloud Fraction profiles from lidar cloud detections***

261 Analyzing CATS lidar echoes lets one identify at which altitude a cloud is present above a  
262 particular location on Earth at a given moment. By aggregating such information over a long  
263 period, vertical profiles of Cloud Fraction can be derived. A CF(z) profile documents at which  
264 frequency clouds were observed at the altitude z over a particular location. Cloud Fractions  
265 are conceptually equivalent to the Cloud Amounts derived from passive measurements

266 (next section) but vertically resolved with a 60 meters resolution.

267 From CATS level 2 data files, we extract profile-based cloud detections and use the  
268 measurement UTC time and coordinates to deduce their local time of observation. Using the  
269 resulting list of cloud layer altitudes, coordinates and local times of detection, we count the  
270 number  $n$  of cloud detected within half-hour bins of local time,  $2^\circ \times 2^\circ$  lat-lon boxes and  
271 200m altitude bins. We also count the number of valid data points  $n_0$  within those bins.  
272 Eventually, we derive the Cloud Fraction  $CF = \frac{n}{n_0}$ , either in individual local time/lat-  
273 lon/altitude bin or by aggregating  $n$  and  $n_0$  over a selection of bins. Thus, we recreate a  
274 statistically accurate representation of the diurnal cycle of Cloud Fractions profiles, over any  
275 location between  $51^\circ\text{S}$  and  $51^\circ\text{N}$ , through the aggregation over long periods of cloud  
276 detections made over that location on different days and local times.

277 CATS reports cloud layers as opaque when no echo from the surface is found in the profile  
278 below a detected cloud, following the same methodology as in Guzman et al., 2017. Below  
279 an opaque cloud layer, there is no laser signal left to propagate, and clouds potentially  
280 present at lower altitudes will not be sampled by the lidar. To account for this effect, we  
281 consider the portions of profiles below an opaque layer unsampled, and they do not count  
282 in the number of valid data points  $n_0$ . This approach limits the influence of laser attenuation  
283 on cloud detections but cannot totally cancel it. For very low clouds (top below 2km), we  
284 make an exception to this rule and consider the lower part of the profile cloudy, as we  
285 found this creates the best agreement with ground-based observations.

286 To enable comparisons with CATS CF profiles (Sect. 3.3 and 4.2), we followed a similar  
287 approach to build CF profiles using cloud detections from SIRTa-reOBS and ARM datasets  
288 (Sect. 2.1), and from CALIPSO Level 2 products (Sect. 2.1.c). In both cases, we counted the  
289 number of cloud detections and valid (non-attenuated) measurements in hourly local time  
290 bins and 200m altitude bins. For CALIPSO, only 01:30AM and PM time bins were filled.

291

### 292 ***b) Building the diurnal cycle of Low and High Cloud Amounts from CATS data***

293 As ISCCP data are based on radiances, clouds therein are characterized according to  
294 their retrieved top pressure  $P$  as low ( $P > 680\text{hPa}$ ), middle ( $440 < P < 680\text{hPa}$ ) or high  
295 ( $P < 440\text{hPa}$ ). To enable a direct ISCCP-CATS comparison, we derived Cloud Amounts (CA)

296 from CATS data for low and high clouds as defined by altitude: low clouds have their top  
297 below 4km ASL, high clouds have their base above 7km, and mid-level clouds are in  
298 between. Using the list of cloud layer altitudes, coordinates and local times of detection  
299 derived from CATS detections (Sect. 2.2.a), we count the number of occurrences  $n'$  of at  
300 least part of one cloud layer in half-hour bins of local time,  $2^\circ \times 2^\circ$  lat-lon boxes and the three  
301 altitude ranges (0-4km, 4-7km and higher than 7km ASL). We also count the number of  
302 occurrences  $n'_0$  that could possibly be reported given the measurements sampled by CATS  
303 within each bin, taking into account the existence of opaque layers. Eventually, we derive  
304 the Cloud Amount  $CA = \frac{n'}{n'_0}$  for low, mid and high-altitude clouds layers, either in individual  
305 local time/lat-lon bin or by aggregating  $n'$  and  $n'_0$  over a selection of bins. Like RS99, we  
306 separated CATS cloud detections over land and ocean, based on the International  
307 Geosphere-Biosphere Programme surface flag present in CATS L2 products on a profile basis  
308 (Palm et al., 2016).

### 309 3. Results

#### 310 3.1. Diurnal Cloud Fraction profiles observed at Global scale

311

312 Figure 1 shows the global diurnal cycle revealed by CATS during JJA from March 2015 to  
313 October 2017 over Ocean and Land (bottom left and right). Low and high clouds are clearly  
314 separated, with a band of minimum cloudiness in-between (near 4km ASL). Above both  
315 surfaces, CATS data show an increase of high clouds during nighttime. Sassen et al. (2009)  
316 explain this increase by the infrared radiative cooling of the upper troposphere. The vertical  
317 spread of high clouds is most narrow near noon, at which point their apparent base is the  
318 highest. These findings are consistent with CALIPSO retrievals (Sassen et al., 2009; Gupta et  
319 al., 2018). The vertical evolution in the fraction of sampled atmosphere due to attenuation  
320 by atmospheric components, for these diurnal cycles and all that follow, is documented in  
321 Appendix C.

322 Significant differences exist between the cloud profiles diurnal cycle above land and ocean.  
323 Clouds generally extend higher over land during nighttime: high clouds are vertically most  
324 frequent near 10km over ocean, while they extend up to 14km above continents until 5AM.  
325 Over ocean, high clouds appear to rise late in the afternoon (3-6PM) and fall soon thereafter  
326 as the sun sets. Land-ocean differences are most striking at low altitudes: over Ocean low  
327 clouds are present almost all day long between 0 and 2km ASL, their CF decreasing from a  
328 20% maximum near 4AM to ~10% between 11AM and 5PM. Over land, low clouds are most  
329 significant during daytime: they appear near 2km ASL at 10AM and extends upwards to  
330 reach 4km ASL near 4PM. The associated CF remains low, at most 8%. These planetary  
331 boundary layer (PBL) clouds are most certainly associated with turbulence and convection  
332 activity occurring near the surface. They disappear after 4PM without connecting to the  
333 higher layers. The clear-sky band (CF < 2%) near the surface is largest at night (almost 2km)  
334 and thinnest in the late morning.

335 An aside on cloud detection: over the ocean, CATS detects more low and high clouds during  
336 nighttime. This means that the increase in high clouds does not prevent the lidar  
337 measurements to represent faithfully at least part of the nocturnal increase in low clouds.

338 During daytime, the decrease in detection sensitivity due to solar pollution could  
339 underestimate the retrieved frequency of clouds (low or high). However, CALIPSO cloud  
340 detections also reveal a nighttime increase in high clouds, which Sassen et al. (2009) and  
341 Gupta et al. (2018) found much too large to be attributed to detection bias from solar noise.  
342 Since CATS daytime cloud detection abilities at 1064nm are at least as good as CALIOP's at  
343 532nm (Yorks et al., 2016), it follows that CATS cloud retrievals should provide a reliable  
344 qualitative assessment of their diurnal cycle, as comparisons with ground-based  
345 measurements will later show (Sect. 3.3). How much solar noise leads to an underestimate  
346 of high clouds in CALIOP and CATS datasets still needs to be quantified.

347 While these seasonal mean results are informative, they mix together unrelated cloud  
348 populations from hemispheres with opposite seasons driven by different circulation  
349 regimes. We thus describe the daily cycles of clouds in zonal bands in the next section.

## 350 **3.2. Diurnal Cloud Fraction profiles observed over mid-latitudes and Tropics**

351 In this section, we consider cloud populations over four latitude bands: midlatitude (30°-  
352 51°) and Tropics (0-30°), in the North Hemisphere (NH) and South Hemisphere (SH), over  
353 land and ocean. We first examine the differences between the diurnal cycles affecting the  
354 cloud vertical profiles over ocean and land in JJA (Sect. 3.2.a and 3.2.b, Fig. 2), then we  
355 discuss how these cycles are affected by the season by considering DJF results (Sect. 3.2.c,  
356 Fig. 3).

357

### 358 *a) High clouds*

359 As expected, Fig. 2 shows that high clouds are located at higher altitude in the tropics (12-  
360 16km ASL) than in midlatitude (8-12km), following the variation of the troposphere depth  
361 with latitude. Also as expected, the occurrence of high clouds is largest (CF > 20%) in deep  
362 convection along the Inter-Tropical Convergence Zone (ITCZ), located between 0° and 30°N  
363 in JJA, and minimum (CF < 8%) in the subsidence branch of the Hadley cell (0°-30°S in JJA). In  
364 mid-latitudes, high clouds (7-9km ASL) are far more frequent (CF ~ 20%) over the Southern  
365 Ocean (30°S-51°S) than over the northern ocean (30-51°N).

366 The CF of oceanic high clouds follows a strong diurnal cycle, with a maximum at nighttime  
367 and a minimum at noon, in mid-latitudes and tropics (even in subsidence region). This cycle  
368 is more pronounced where the high clouds are more numerous: along the ITCZ (0-30°N) and  
369 in the Southern Ocean (30-51°S). In addition to the variation in the high cloud occurrence,  
370 the vertical distribution of these clouds also follows a marked diurnal cycle along the ITCZ:  
371 detections spread vertically over more than 4km near midnight, but over less than 1km at  
372 noon. This spreading out occurs between 5PM and 10PM, and disappears much faster  
373 during the morning. A wider spread of detection altitudes can either indicate the presence  
374 of geometrically thicker clouds, or a wider distribution of optically thick clouds tops only  
375 partially sampled by CATS. By comparison, over the Southern Ocean high cloud detections  
376 occur over the same altitude range throughout the day.

377 Overall, high clouds behave very similarly above land (Fig. 2, right column) and ocean (Fig. 2,  
378 left column) at all latitudes, except between 30-51°S where the continental surface is too  
379 small to conclude.

380

381 *b) Low clouds*

382 Over ocean in JJA (Fig. 2), the occurrence of low clouds (0-3km ASL) changes significantly  
383 with latitude: The Southern Ocean region (30-51°S) is by far the cloudiest, the mid-latitude  
384 north (30-51°N) and the subsidence tropics (0-30°S) are moderately cloudy, and even less  
385 low clouds are observed along the ITCZ (0-30°N). The oceanic low clouds show only small  
386 variations along the day. A weak diurnal cycle occurs at all latitudes except along the ITCZ  
387 (possibly because low clouds there are in part masked by higher clouds affected by an out-  
388 of-phase diurnal cycle). Low-level clouds are more numerous in nighttime (CF near 20%)  
389 compared to daytime (CF~12%) in subsidence tropics (0-30°S) and mid-latitude north (30-  
390 51°N). The southern oceanic low clouds exhibit a very faint diurnal cycle: their CF gets over  
391 20% nearly all day long, with a very small decrease near 2PM.

392 In contrast to high clouds, the differences between land and ocean are striking for the low  
393 and mid-level clouds. Both the occurrences and the diurnal cycles of clouds over land differ  
394 significantly from their oceanic counterparts. The low clouds are very few over land (CF~4%)  
395 compared to over ocean (>16%), all day long. Moreover, the continental low cloud diurnal  
396 cycle exhibits a maximum in the early afternoon (around 2PM) that does not show up over  
397 ocean: a maximum CF appears around 2.5 km of altitude in the upper edge (or just above  
398 the top) of the atmospheric boundary layer; it is linked to convective activity between 10AM  
399 and 5PM.

400 Another noticeable difference between land and ocean is the presence of well-defined mid-  
401 level cloud population over NH tropical land (0-30°N, 2nd row on the right in Fig. 2) in the  
402 free troposphere between 5 and 7 km ASL. These mid-level clouds show a diurnal cycle  
403 opposite to PBL clouds and similar to the high clouds in that its minimum occurs at midday  
404 and its maximum at night, although the magnitude of this cycle is much more limited. This  
405 altitude range would be consistent with cumulus congestus (Johnson et al., 1999). Those,  
406 however, are present above both land and ocean (Masugana et al. 2005) and CATS finds little  
407 clouds at these altitudes over ocean. Rather, the clouds altitudes and location, over land in  
408 the summer hemisphere, are consistent with Altocumulus clouds as described by Sassen and  
409 Wang (2012) using CALIPSO and CloudSat measurements. Bourgeois et al. (2017) discussed  
410 the diurnal cycle of similar clouds observed over West Africa: they found these clouds reach



411 maximum occurrence early in the morning, which is consistent with our results.

412

### 413 *c) Seasonal differences*

414 Figure 3 presents diurnal cycles of Cloud Fraction profiles over the same latitude bands as  
415 Fig. 2 but based on data collected during the boreal winter (DJF). As seasons switch  
416 hemispheres, we anticipate cloud populations to undergo symmetric changes across  
417 hemispheres, in agreement with large-scale dynamic processes driving their spatial  
418 distribution on seasonal time scales. This is verified for high clouds (Fig. 2 vs. Fig. 3): in the  
419 Tropics the ITCZ moves to South and with it the large CF at high altitudes, in midlatitudes the  
420 high clouds are more frequent during the winter season, due to more frequent low-pressure  
421 conditions.

422 Interestingly, the mid-altitude clouds visible near 6km ASL in the NH Tropics over land (Fig. 2,  
423 2nd row on the right) also move to the SH Tropics in DJF (Fig. 3, 3rd row on the right). This  
424 confirms the year-long persistence of midlevel clouds over continental tropical regions found  
425 by Bourgeois et al. (2017).

426 The seasonal changes in low clouds are less symmetric than in higher clouds, as they are  
427 more closely related to surface conditions. Over ocean, in DJF the amount of low clouds  
428 increases dramatically in NH midlatitudes compared to JJA (Fig. 2 and 3, top left), but does  
429 not change noticeably in the SH midlatitudes: the diurnal cycle that sees a slight decrease in  
430 the huge population of low clouds over the Southern Ocean is present in both seasons (Fig.  
431 2 and 3, bottom left). Over land, in the Tropics, low clouds appear similar in frequency and  
432 behavior in both DJF and JJA: PBL clouds extend vertically between ~7AM to 5PM (Fig. 2 and  
433 3, rows 2 and 3 of right column). The NH midlatitudes show the strongest seasonal change in  
434 low clouds, as they become present all day long: the diurnal cycle associated with PBL  
435 development in JJA disappears in DJF (Fig. 2 and 3, top right). SH midlatitude retrievals over  
436 land are noisy in DJF and JJA, but the DJF data (Fig. 3, bottom right) suggests that low clouds  
437 there extend vertically a lot more than in JJA, up to 4km ASL.

### 438 **3.3. Diurnal cycle of cloud profiles above selected continental regions**

439

440 In this section, our first goal is to compare the diurnal cycle of the Cloud Fraction profiles  
441 from CATS against independent observations collected by active instruments from ground-  
442 based sites (Sect. 3.3.a and 3.3.b). In particular, we want to understand if the behaviors  
443 found so far (Fig. 1-3) are valid for low clouds despite the attenuation of the space laser  
444 signal (Sect. 2.2.a). Our second goal is to compare, for the first time, the diurnal cycle of the  
445 Cloud Fraction profiles over different continental regions all over the globe as observed with  
446 a single instrument (Sect. 3.3.c).

447 It is important to note that since detection sensitivity, penetration depths and algorithmic  
448 choices (e.g. averaging times and distances) change significantly from one instrument to the  
449 next, we do not expect the various datasets to agree on absolute values of Cloud Fraction  
450 profiles or Cloud Amounts. Rather, our interest is in whether different instruments agree on  
451 the behavior of the diurnal evolution of clouds when they document the same location.  
452 Thus the following comparison focus on the main features of the daily cycles and not on  
453 absolute values.

454

#### 455 ***a) Over South of Paris in Europe***

456 Figure 4 shows the diurnal evolution of CF profiles seen by the ground-based LNA lidar (top  
457 left) operated on the SIRTA site south of Paris (Sect. 2.1.b) and seen by CATS in a 10°x10°  
458 box centered on SIRTA, keeping only profiles sampled over land (top right). Both datasets  
459 report a well-defined high-altitude layer, with a clear-cut cloud top near 12 km ASL that  
460 rises up a few hundred meters in the morning until 10AM and slowly falls during the  
461 afternoon by at most 1 km. In both figures, the bottom of this layer is not sharply defined:  
462 the CF decreases almost linearly from 11-12km ASL to near-zero at 4km ASL. Both  
463 instruments also report a low-level cloud layer that initiates in the morning and extends  
464 upwards from ~1km ASL at 5AM to ~4km ASL near 8PM.

465 Regarding differences, CATS sees more high-altitude clouds. In the late afternoon (starting  
466 near 5PM), in particular, the ground-based lidar instead sees much less high clouds; that  
467 instrument, however, suffers from poor sampling at this late hour. CATS reports less

468 boundary layer clouds, particularly in the late afternoon, when the ground-based lidar  
469 reports low-level CF above 20% (again, a time of poor sampling). The large number of high-  
470 altitude clouds observed by CATS at that time could impair its ability to detect lower clouds,  
471 while at the same time the many low clouds observed by the ground lidar can impair its  
472 ability to detect high clouds. The absence of precipitating clouds from the LNA dataset could  
473 also explain this difference.

474

#### 475 ***b) Over the US Southern Great Plains ARM site***

476 Figure 4 shows the diurnal evolution of CF profiles seen by the SGP-based radar (2nd row,  
477 left) and CATS (right) in a 10°x10° lat-lon box centered on the SGP site (Sect. 2.2.b), keeping  
478 only profiles sampled over land. During nighttime, both datasets report frequent high-level  
479 clouds near 12km ASL, with large CF between 16:00 and 03:00 LT. At night, high clouds are  
480 also more distributed vertically, between 9 and 14km ASL. CATS and SGP datasets agree that  
481 the importance of high-level clouds strongly drops during daytime (7AM-5PM), with a  
482 minimum CF at midday. During daytime, the vertical distribution of high-level clouds is more  
483 narrow, from 11 to 12km ASL at its thinnest point (near 10AM). This rather strong cycle of  
484 high-level clouds can be explained by possible influence from Tropical dynamics at the 36°N  
485 latitude of the SGP site. There are slightly more midlevel clouds (4-8km ASL) at night, with  
486 increasing CF between midnight and 7AM. PBL clouds form near the surface at 9AM, rise  
487 and thicken almost up to 4km ASL near 4PM.

488 There are of course differences. The SGP radar detects PBL and midlevel clouds twice more  
489 frequently than CATS, even though few high clouds are present. CATS also misses low-level  
490 clouds observed by the SGP radar between 6PM and 6AM, probable stratiform clouds that  
491 could either be too optically thin for CATS or miscategorized by its cloud detection  
492 algorithm.

493

#### 494 ***c) Over the subtropical Eastern North Atlantic ARM site***

495 Figure 4 shows the diurnal evolution of CF profiles seen by the ENA-based radar (bottom  
496 row, left) and CATS (right) in a 10°x10° lat-lon box centered on the ENA site (Sect. 2.2.b). The  
497 vertical distribution of clouds appears very different over this oceanic site. Both CATS and

498 the ENA radar agree on the day-long persistence of low-level clouds below 2km ASL, and on  
499 their slight drop in Cloud Fraction and vertical spread between noon and 6PM. This is  
500 consistent with persistent stratiform clouds that are maximum at night. CATS sees more  
501 high clouds (8-12km ASL) than the ENA radar (4-12km ASL). CATS also reports a Cloud  
502 Fraction minimum between 0300-0500LT that is not present in ground-based dataset.

503 These three comparisons between CATS and ground-based measurements suggest that, in  
504 general, the spaceborne lidar sees more high-level clouds and the ground-based instrument  
505 more low-level clouds. This sampling bias affects all space lidar comparisons with ground  
506 instruments (e.g. Dupont et al., 2010). Even so, we find similar behavior in the diurnal cycles  
507 reported by CATS and ground instruments over the same locations. Dataset discrepancies  
508 appear acceptable given the much smaller size of the CATS dataset (infrequent overpasses  
509 over 3 seasons compared to daily local measurements) and the instrumental and  
510 algorithmic variations already mentioned. It is reassuring to find that CATS results retain the  
511 major features of the clouds profile daily cycle, most notably an acceptable representation  
512 of the daytime low-level boundary layer clouds at all three sites despite the presence of  
513 high-level clouds.

514 In this section, we have seen that retrievals from ground-based instruments suggest CATS  
515 measurements reliably document the clouds diurnal cycle. Due to the distribution of  
516 ground-based sites, however, this approach is limited to mostly midlatitudes from the  
517 Northern Hemisphere. Next, we compare CATS detections with global spaceborne  
518 retrievals.

519

#### 520 ***d) Diurnal cycles of the cloud profiles over continents***

521 Continents are diverse in ground type, orography, latitude, exposition to large-scale  
522 atmospheric circulation, and transport of air masses from the local environment. These  
523 factors influence the atmosphere above the continent, leading to possible variations in the  
524 cloud diurnal cycle profiles. Ground-based observations let us document these different  
525 cycles, but differences between instruments and operations in the different ground sites  
526 make comparing diurnal cycle observed from ground at different locations difficult. Thanks  
527 to CATS data, for the first time we compare here the cloud diurnal cycle profiles observed  
528 over different continents by a single instrument and with a relatively large space sampling,

529 compared to single-site ground-based observations. Figure 5 illustrates how the diurnal  
530 cycle of CF varies among seven large continental areas across both hemispheres, considering  
531 only cloud detections made by CATS over land within lat-lon boxes (defined in the inset map)  
532 during the summer seasons (JJA in the NH, DJF in the SH).

533 During summer most continents share a development of PBL clouds during sunlit hours  
534 (with similar Cloud Fractions, hours and vertical extents), except NH Africa where low clouds  
535 are almost absent. Most continents also share a nighttime maximum and daytime maximum  
536 of high clouds, with an associated narrowing of their vertical distribution during morning  
537 and a spreading out during the afternoon. Variations in cloudiness and cloud vertical  
538 distribution are particularly intense over South America and SH Africa, while they are  
539 minimal over Australia. A mid-altitude cloud layer is present almost all day long, with a faint  
540 daytime minimum, over all SH continents and NH Africa.

541 Note that the present comparison is less robust in the lower troposphere than higher in the  
542 troposphere, due to the attenuation of the space lidar signal as it penetrates the  
543 atmosphere.

544

545 **4. Discussion**

546

547 Hereafter we use our results for answering the following questions: How does the diurnal  
548 cycle of low, mid, high cloud covers from geostationary satellites compare with CATS ones?  
549 Do the existing lidar space missions document extreme or average behaviors of the cloud  
550 profile diurnal cycle? What about upcoming sun-synchronous lidar space missions?

551

552 **4.1 About the Diurnal cycles of Low and High Cloud Amounts**

553

554 CATS observations provide an opportunity to compare the cloud diurnal cycle derived from  
555 the ISCCP dataset (Sect. 2.1.c) with completely independent observations at near-global  
556 scale (excluding latitudes higher than 51°). In particular, we expect cloud retrievals from an  
557 active sensor such as CATS to be independent of the surface, even above highly reflective  
558 surfaces such as ice and deserts and to include optically thin clouds. Since CATS sampling is  
559 constrained between 51°S and 51°N, its data cannot be used to document the diurnal cycle  
560 in the polar regions, like ISCCP does: our comparison will extend at most to midlatitudes.  
561 Figure 6 shows the diurnal cycle of the Low and High cloud covers observed by the CATS  
562 space lidar.

563 Over ocean CAs are very stable, the diurnal cycle is almost flat (Fig. 6, left column). CATS  
564 shows a weak cycle for low clouds, with a maximum in mid-morning and a minimum in  
565 early-afternoon, which is also visible in ISCCP data. For oceanic high clouds, CATS exhibit  
566 almost no diurnal cycle except in the Tropics where they follow the same cycle as low  
567 clouds. ISCCP also shows a weak cycle for high clouds, but opposite to the CATS one. This  
568 might be related to the fact that CATS can detect optically thin high clouds better than  
569 ISCCP. The optically thicker high clouds seen by ISCCP are thus probably more linked to deep  
570 convection activity. CATS can better detect optical thin high clouds, which should be more  
571 decoupled from convection and less affected by diurnal cycles.

572 Over land, between 15°S and 51°N, CATS reports that low-clouds have a pronounced diurnal  
573 cycle with a maximum of low-level clouds at midday (+10%) and a minimum at midnight (-  
574 5%). This is consistent with ISCCP observations (Figure 11 in RS99), but in the Northern mid-

575 latitudes the amplitude of the cycle is weaker for CATS than ISCCP (minimum at -4% instead  
576 of -12%). For high-level clouds over land in the Tropics (15°S-30°N) CATS observes a  
577 maximum during night-time and a minimum at noon; the timing is consistent with ISCCP but  
578 the amplitude is slightly more pronounced with CATS than ISCCP (-12% instead of -7% at  
579 midday). In the Southern hemisphere (15°S-51°S) the similarity between CATS and ISCCP  
580 gets lost, probably because the land surface is small in those latitude ranges and the  
581 observations are not significant.

582 In summary, CATS confirms the shape of the Low and High cloud diurnal cycles observed by  
583 ISCCP except for high tropical clouds. This could be due to the space lidar detecting a larger  
584 number of optically thinner clouds not directly linked to deep convection, or to the different  
585 day-night cloud detection sensitivities of active and passive measurements. In most cases,  
586 the amplitudes of the diurnal cycle observed by CATS differ from those observed by ISCCP.

587 Both CATS and ISCCP miss some low clouds that are masked by the presence of high thick  
588 clouds. So even if CATS and ISCCP diurnal cycles are roughly consistent in low clouds, both  
589 results might be biased in the same direction. The high clouds diurnal cycle presented here  
590 are more robust than the low clouds ones.

591

## 592 **4.2 About the Cloud Fraction profiles observed at fixed local times by space lidars**

593 The CALIOP lidar has provided detailed Cloud Fraction profiles since 2006 at 0130AM and  
594 0130 PM LT. The next spaceborne atmospheric lidar missions ADM-Aeolus, to be launched  
595 in late 2018 (Culoma et al., 2017) on a sun-synchronous orbit, will enable measurements at  
596 0600AM and 0600PM LT. After that, the ATLID lidar on the Earth-CARE platform (Illingworth  
597 et al., 2015), expected to launch in 2020, will operate at fixed local times close to CALIOP  
598 (02:00AM and PM). The CATS dataset may remain for the near future our single source of  
599 diurnally distributed cloud profile lidar measurements from space.

600

### 601 *a) Comparison between CATS and CALIPSO*

602 In this section, we first check how CATS sees the day/night variation in cloud profiles also  
603 documented by CALIOP through its two daily overpasses. Figure 7 shows vertical profiles of

604 Cloud Fraction reported by both datasets at 0130AM and PM, over ocean (left) and land  
605 (right), latitude-weighted and averaged between 51°S and 51°N over JJA between 2015 and  
606 2017. The black lines show the CF obtained when considering all measurements from both  
607 instruments. Over land and ocean, we find that both CALIPSO and CATS overall report larger  
608 Cloud Fractions at 0130AM (blue) than 0130PM (red), in agreement with the findings of  
609 Gupta et al. (2018). Below 2.5 km, this difference is stronger over ocean (+7% in 0130AM  
610 CF) than over land. Both datasets report a strong increase in 0130AM CF (almost +7%  
611 compared to 0130PM) above 15km over land.

612 The CF profiles reported by both datasets agree very well over Ocean (left) in both daytime  
613 and nighttime conditions. Over land (right) in daytime (red) conditions, CATS reports slightly  
614 more low-level clouds (CF~7% near 1km ASL, ~5% for CALIOP). This difference, which is  
615 present at all latitudes above land during daytime (not shown), might be due to the so-  
616 called single-shot low clouds, for which CALIOP data undergoes a specific processing  
617 (Winker et al., 2009). The strongest differences appear for nighttime CF over land (right,  
618 blue): CALIPSO CF is larger than CATS CF by a 2-3% throughout the entire profile. A perfect  
619 agreement between CF from both datasets should not be expected, as the CATS and CALIOP  
620 lidars operate in different configurations – wavelengths, pulse repetition frequencies and  
621 signal-to-noise ratios are different, for a start. These technical variations lead to differences  
622 in, for instance, how fast the laser pulse energy of both instruments gets attenuated as it  
623 penetrates atmospheres of various compositions, or differences in cloud detection  
624 performance, e.g. when sampling optically thin clouds in the upper troposphere, or  
625 fractionated boundary layer clouds (see Reverdy et al., 2015 for a study of the impact of  
626 design choices on lidar retrievals). Both datasets agree quite well on the general vertical  
627 pattern of the profile, though. A useful conclusion is that considering CALIPSO observations  
628 at both overpass local times (i.e. 0130AM and 0130PM) apparently provides a good  
629 approximation of the daily average Cloud Fraction profile.

630

631 b) Comparison of Cloud Fraction profiles at various times of satellite overpass

632 As a final analysis, we represent the range covered by CATS hourly CF profiles over a day  
633 (averaged over the globe - white envelope in Fig. 8) and show CF profiles observed by CATS  
634  $\pm 1$  hour around the fixed local observation times of the three sun-synchronous space lidar



635 missions (CALIPSO, ADM-Aeolus, EarthCare).

636 Our first aim is to understand how wind observations made at fixed local time by ADM-  
637 Aeolus might be impacted by the cloud diurnal cycle. ADM-Aeolus will provide information  
638 on wind only in absence of clouds. Figure 8 indicates that ADM-Aeolus overpass times are  
639 quite cloudy in both AM and PM compared to the diurnal variability (white envelope). The  
640 PM overpass corresponds to the daily maximum in cloud profiles over both ocean and land,  
641 while AM observations correspond to a time representative of the daily average Cloud  
642 Fraction profile. As more clouds occur in the PM than AM observations, less wind  
643 information will likely be provided by ADM-Aeolus in the afternoon than in the morning. For  
644 the future, another ADM-Aeolus-like mission around midday (minimum Cloud Fraction  
645 profile) would increase the number of wind measurement with respect to the cloud  
646 occurrence.

647 Our second aim is to understand how well observations made at fixed local times by space  
648 lidar dedicated to clouds studies (CALIPSO and EarthCare) capture the daily variability of  
649 Cloud Fraction profiles. Figure 8 suggests that over land (right), CALIPSO and Earth-CARE  
650 retrievals capture only part of the daily CF variability above 8km ASL: the PM measurements  
651 overestimate the daily CF minima and the AM measurements underestimate the daily CF  
652 maxima. Below 8km ASL they are rather representative of the daily average, except below  
653 5km ASL where PM measurements get close to the daily CF maxima. Figure 8 also shows  
654 that over Ocean (left) CALIPSO and Earth-CARE retrievals should be considered as the daily  
655 CF maxima during the nighttime (AM) overpass and as the daily CF minima during the  
656 daytime (PM) overpass. This has interesting implications: it suggests that not only CALIPSO  
657 but all the observations dedicated to cloud studies collected by the instruments within the  
658 A-train (CloudSat, CERES, MODIS, PARASOL, etc.) have documented the state of the  
659 atmosphere in the extreme states of the cloud profile diurnal cycle over the last 12 years  
660 over ocean. These conclusions suggest the A-Train observations are likely relevant and  
661 robust to constrain the cloud diurnal cycle extremes in climate models and climate studies.

662

663

664 **5. Conclusions**

665 In this paper, we took advantage of the variable local time of overpass of the International  
666 Space Station to document the diurnal cycle of the cloud vertical profile as seen by the CATS  
667 lidar. This is the first time the diurnal evolution of the vertical cloud profile is documented on  
668 that vertical scale on a large part of the globe, between 51°S and 51°N. Our results are based  
669 on 15 months of systematic observations (3 boreal summers and 2 austral summers)  
670 collected during the 2015-2017 time period, which enable statistically significant results.

671 The main results follow. We observed that high tropical clouds begin to spread out vertically  
672 in the late afternoon (4-5PM). Their vertical distribution is largest (over 5km) near 10PM.  
673 This spread-out is particularly large in the Summer Hemisphere in DJF. A mid-level cloud  
674 layer (4-8 km ASL) persists all day long over the tropical continent during summer, with a  
675 weak diurnal cycle (minimum at noon). Southern Ocean results are quite unique; low clouds  
676 (0-2km ASL) cover this ocean all day long in summer and winter. A slight diurnal cycle sees  
677 their CF drop by a few percents during the afternoon (from noon to 6PM), but their vertical  
678 distribution stays constant. High clouds are also frequent over the Southern Ocean, more so  
679 in JJA. They follow a diurnal cycle in summer and winter, with an daytime minimum (from  
680 8AM and 3PM). At all latitudes, continental low clouds are most frequent in the early  
681 afternoon (around 2PM) at about 2.5 km ASL. Finally, our results show that in summer the  
682 diurnal cycle of continental clouds is similar in both hemispheres: a rapid development of  
683 near-surface PBL clouds during sunlit hours, and an increase in cloudiness and wider vertical  
684 distributions during nighttime for high-altitude clouds (stronger over the SH and the  
685 Tropics). Exceptions are NH Africa, where PBL clouds are very few, and Australia, where high  
686 clouds appear only significant between 8 and 11PM.

687 We evaluated the diurnal cycle derived from CATS against independent ground-based  
688 observations and found satisfactory agreement. Moreover, our results suggest that over  
689 oceans CALIPSO and Earth-CARE should describe the daily minimum of the Cloud Fraction  
690 profile during their PM overpass, and its daily maximum during their AM overpass. This  
691 supports the idea that data collected by A-train instruments (not only CALIPSO) are very  
692 relevant to document the cloud diurnal cycle. This is also roughly the case over land at  
693 altitudes above 8km ASL, although the amplitude of the diurnal variability is quite  
694 underestimated.

695 Questions remain about how several factors could affect our ability to retrieve the vertical  
696 variability of clouds from lidar-based measurements through the day. More specifically, the  
697 irruption of solar noise in daytime conditions requires increased horizontal averaging to  
698 keep CATS detection sensitivity stable. High clouds with very small optical depths (lower  
699 than 0.005), which CATS can detect in the nighttime, will be probably missed in the daytime.  
700 Meanwhile, the occurrence and extent of fragmented boundary layer clouds might be  
701 overestimated. Even though prior work using the similarly-affected CALIPSO data suggests  
702 the observed diurnal changes in clouds are too large to be solely due to those effects, their  
703 impact on the retrieved cycles needs to be quantified. In the same manner, how extinction  
704 by high clouds impacts the retrieved Cloud Fractions at low altitude needs to be  
705 investigated.

706 In the future, it would be possible to consider CATS measurements at smaller scales, to  
707 identify regionally consistent cloud populations and diurnal behaviors over specific regions  
708 of interest. It would also be possible to use CATS detection of opaque cloud layers to identify  
709 the best local time of observation from space to study local cloud radiative effects. We will  
710 address these lines of research in upcoming papers.

## 711 **Acknowledgments**

712 CATS and CALIPSO data were obtained through the NASA Langley Research Atmospheric  
713 Science Data Center (ASDC) and the AERIS and ICARE/CGTD Data services. ARM-ENA and  
714 ARM-SGP data were obtained through the ARM portal at <http://www.arm.gov>, SIRTA data  
715 were obtained through the ReOBS portal at <http://sirta.ipsl.fr/reobs.html>. Data were  
716 analyzed on the Climserv IPSL computing facilities. This research was made possible through  
717 support by CNRS and CNES. We want to thank J.-L. Baray and N. Montoux for useful  
718 discussions.

719 **References**

720

- 721 • Ackerman, T. P., and G. M. Stokes (2003), The Atmospheric Radiation Measurement  
722 Program Phys. Today, 56, 38–44, doi:10.1063/1.1554135
- 723 • Bouniol, D., R. Roca, T. Fiolleau, and D.E. Poan, 2016: [Macrophysical, Microphysical,  
724 and Radiative Properties of Tropical Mesoscale Convective Systems over Their Life  
725 Cycle](#). *J. Climate*, **29**, 3353–3371, [doi:10.1175/JCLI-D-15-0551.1](#)
- 726 • Bourgeois, E., D. Bouniol, F. Couvreux, F. Guichard, J. H. Marsham, L. Garcia-Carreras,  
727 C. E. Birch, and D. J. Parker (2018), Characteristics of mid-level clouds over West  
728 Africa, *QJRM*S, **113**, D04210–17, doi:10.1002/qj.3215.
- 729 • Ceppi, P., F. Briant, M. D. Zelinka, and D. L. Hartmann, 2017: Cloud feedback  
730 mechanisms and their representation in global climate models, *WIREs Climate  
731 Change* 2017, e465. Doi: 10.1002/wcc.465
- 732 • Cesana, G., and H. Chepfer (2013), Evaluation of the cloud thermodynamic phase in a  
733 climate model using CALIPSO-GOCCP, *J. Geophys. Res.*, **118**(14), 7922–7937,  
734 doi:10.1002/jgrd.50376.
- 735 • Cesana, G., H. Chepfer, D.M. Winker, B. Getzewich, X. Cai, H. Okamoto, Y. Hagihara, O.  
736 Jourdan, G. Mioche, V. Noel, M. Reverdy, 2016: Using in situ airborne measurements  
737 to evaluate three cloud phase products derived from CALIPSO, *J. Geophys. Res.*  
738 *Atmos.*, **121**, 5788–5808, doi:10.1002/2015JD024334
- 739 • Chepfer, H., Bony, S., Winker, D., Cesana, G., Dufresne, J. L., Minnis, P., Stubenrauch,  
740 C. J. and Zeng, S.: The GCM-Oriented CALIPSO Cloud Product (CALIPSO-GOCCP), *J.*  
741 *Geophys. Res.*, **115**(1), 23073–13, doi:10.1029/2009JD012251, 2010.
- 742 • Chepfer H., G. Cesana, D. Winker, B. Getzewich, and M. Vaughan, 2013: Comparison  
743 of two different cloud climatologies derived from CALIOP Level 1 observations: the  
744 CALIPSO-ST and the CALIPSO-GOCCP, *J. Atmos. Ocean. Tech.*, doi.10.1175/JTECH-D-  
745 12-00057.1
- 746 • Chiriaco M., S. Bastin, P. Yiou, M. Haeffelin, J.-C. Dupont, L. Klenov, M. Stéfanon,  
747 2014: European heat-wave in July 2006: observations and modelling showing how

- 748 local processes amplify conducive large-scale conditions. *Geophys. Res. Let.*, 41 issue  
749 15, 5644 – 5652.
- 750 • Chiriaco, M., Dupont, J.-C., Bastin, S., Badosa, J., Lopez, J., Haeffelin, M., Chepfer, H.,  
751 and Guzman, R.: ReOBS: a new approach to synthesize long-term multi-variable  
752 dataset and application to the SIRTA supersite, *Earth Syst. Sci. Data*, 10, 919-940,  
753 <https://doi.org/10.5194/essd-10-919-2018>, 2018
  - 754 • Culoma A., A. Elfving, R. Meynart, A. Straume, D. Wernham, "AEOLUS mission: the  
755 latest preparations before launch", *Proc. SPIE 10423, Sensors, Systems, and Next-*  
756 *Generation Satellites XXI*, 1042303 (29 September 2017); doi: 10.1117/12.2282159
  - 757 • Dong, X., B. Xi, K. Crosby, C. N. Long, R. S. Stone, and M. D. Shupe (2010), A 10 year  
758 climatology of Arctic cloud fraction and radiative forcing at Barrow, Alaska, *J.*  
759 *Geophys. Res.*, 115(D17), D17212, doi:10.1029/2009JD013489.
  - 760 • Dupont, J. C., M. Haeffelin, Y. Morille, V. Noel, P. Keckhut, D. Winker, J. Comstock, P.  
761 Chervet, and A. Roblin (2010), Macrophysical and optical properties of midlatitude  
762 cirrus clouds from four ground-based lidars and collocated CALIOP observations, *J.*  
763 *Geophys. Res.*, 115(D4), D00H24–15, doi:10.1029/2009JD011943.
  - 764 • Elouragini, S. and Flamant, P. H.: Iterative method to determine an averaged lidar  
765 ratio and the range resolved extinction in cirrus, *Appl. Opt.*, 35, 1512–1518, 1996.
  - 766 • Gray, W. M., and R. W. Jacobson, 1977: Diurnal variation of deep cumulus convection.  
767 *Mon. Wea. Rev.*, 105, 1171–1188, doi:10.1175/1520-  
768 0493(1977)105,1171:DVODCC.2.0.CO;2
  - 769 • Greenwald, T. J. and Christopher, S. A.: Daytime variation of marine stratocumulus  
770 microphysical properties as observed from geostationary satellite, *Geophysical*  
771 *Research Letters*, 26(1), 1723–1726, doi:10.1029/1999GL900346, 1999.
  - 772 • Guzman, R., H. Chepfer, V. Noel, T. Vaillant de Guélis, J. E. Kay, P. Raberanto, G.  
773 Cesana, M. A. Vaughan, and D. M. Winker (2017), Direct atmosphere opacity  
774 observations from CALIPSO provide new constraints on cloud-radiation interactions,  
775 *J. Geophys. Res.*, 1–20, doi:10.1002/2016JD025946.
  - 776 • Haeffelin, M. et al. (2005), SIRTA, a ground-based atmospheric observatory for cloud

- 777 and aerosol research, *Annales Geophysicae*, 23(2), 253–275, doi:10.5194/angeo-23-  
778 253-2005.
- 779 • Haynes, J. M., T. H. Vonder Haar, T. L'Ecuyer and D. Henderson (2013) Radiative  
780 heating characteristics of earth's cloudy atmosphere from vertically resolved active  
781 sensors. *Geophys Res Lett* 40:624–904 630. doi:10.1002/grl.50145.
  - 782 • Hoareau, C., P. Keckhut, V. Noel, H. Chepfer, and J. L. Baray (2013), A decadal cirrus  
783 clouds climatology from ground-based and spaceborne lidars above the south of  
784 France (43.9° N–5.7° E), *Atmos. Chem. Phys.*, 13(14), 6951–6963, doi:10.5194/acp-  
785 13-6951-2013.
  - 786 • Hogan, R. J., A. J. Illingworth, E. J. O'Connor, and J. P. V. Poiares Baptista (2003),  
787 Characteristics of mixed-phase clouds. II: A climatology from ground-based lidar,  
788 *QJRMS*, 129, 2117–2134.
  - 789 • Hu, Y. et al. (2009), CALIPSO/CALIOP Cloud Phase Discrimination Algorithm, *J. Atmos.*  
790 *Oceanic Technol.*, 26, 2293–2309.
  - 791 • Illingworth, A. J. et al. (2015), The EarthCARE Satellite: The Next Step Forward in  
792 Global Measurements of Clouds, Aerosols, Precipitation, and Radiation, *Bull. Am.*  
793 *Met. Soc.*, 96(8), 1311–1332, doi:10.1175/BAMS-D-12-00227.1.
  - 794 • Johnson, R. H., T. M. Rickenbach, S. A. Rutledge, P. E. Ciesielski, and W. H. Schubert  
795 (1999), Trimodal Characteristics of Tropical Convection, *J. Climate*, 12(8), 2397–2418,  
796 doi:10.1175/1520-0442(1999)012<2397:TCOTC>2.0.CO;2.
  - 797 • Kato, S., F. G. Rose, S. S. Mack, W. F. Miller, and co-authors (2011), Improvements of  
798 top-of-atmosphere and surface irradiance computations with CALIPSO-, CloudSat-,  
799 and MODIS-derived cloud and aerosol properties. *J Geophys Res* 116:D19209.  
800 doi:10.1029/2011JD016050
  - 801 • Kollias, P., Bharadwaj, N., Widener, K., Jo, I. and Johnson, K.: Scanning ARM Cloud  
802 Radars. Part I: Operational Sampling Strategies, *J. Atmos. Oceanic Technol.*, 31(3),  
803 569–582, doi:10.1175/JTECH-D-13-00044.1, 2014.
  - 804 • Konsta, D., J. L. Dufresne, H. Chepfer, A. Idelkadi, and G. Cesana (2016), Use of A-train  
805 satellite observations (CALIPSO–PARASOL) to evaluate tropical cloud properties in the

- 806 LMDZ5 GCM, *Clim. Dyn.*, 1–22, doi:10.1007/s00382-015-2900-y.
- 807 • Kummerow, C., W. Barnes, T. Kozu, J. Shiue, and J. Simpson (1998), The Tropical  
808 Rainfall Measuring Mission (TRMM) sensor package, *J. Atmos. Oceanic Technol.*, 15,  
809 809–817.
- 810 • L'Ecuyer, T. S., N. B. Wood, T. Haladay, G. L. Stephens, and P. W. Stackhouse  
811 Jr. (2008), Impact of clouds on atmospheric heating based on the R04 CloudSat fluxes  
812 and heating rates data set, *J. Geophys. Res.*, 113, D00A15,  
813 doi:[10.1029/2008JD009951](https://doi.org/10.1029/2008JD009951).
- 814 • L'Ecuyer, T. S., and J. H. Jiang, 2010: Touring the atmosphere aboard the A-Train.  
815 *Physics Today*, vol .63 (7), 36-40.
- 816 • Liu, Z., M. A. Vaughan, D. Winker, C. Kittaka, B. Getzewich, R. Kuehn, A. Omar, K. A.  
817 Powell, C. Trepte, and C. Hostetler (2009), The CALIPSO lidar cloud and aerosol  
818 discrimination: Version 2 algorithm and initial assessment of performance, *J. Atmos.*  
819 *Oceanic Technol.*, 26, 1198–1213.
- 820 • Masunaga, H., T.S. L'Ecuyer, and C.D. Kummerow, 2005: [Variability in the](https://doi.org/10.1175/JCLI-3304.1)  
821 [Characteristics of Precipitation Systems in the Tropical Pacific. Part I: Spatial](https://doi.org/10.1175/JCLI-3304.1)  
822 [Structure](https://doi.org/10.1175/JCLI-3304.1). *J. Climate*, 18, 823–840, <https://doi.org/10.1175/JCLI-3304.1>
- 823 • McGill, M. J., J. E. Yorks, V. S. Scott, A. W. Kupchok, and P. A. Selmer (2015), The  
824 Cloud-Aerosol Transport System (CATS): A technology demonstration on the  
825 International Space Station, *Proc. SPIE 9612, Lidar Remote Sensing for Environmental*  
826 *Monitoring XV*, 96120A, doi:10.1117/12.2190841.
- 827 • Naud, C., Del Genio, A. D., Haeffelin, M., Morille, Y., Noel, V., Dupont, J.-C., Turner, D.,  
828 Lo, C., and Comstock, J. M., 2010: Thermodynamic phase profiles of optically thin  
829 midlatitude clouds and their relation to temperature. *J. Geophys. Res.*, 115 D11202
- 830 • Noel, V. and Haeffelin, M., 2007: Midlatitude Cirrus Clouds and Multiple Tropopauses  
831 from a 2002-2006 Climatology over the SIRTA observatory. *J. Geophys. Res.*, 112  
832 D13206
- 833 • Wang, Z., and K. Sassen, 2001: Cloud type and macrophysical property retrieval using  
834 multiple remote sensors. *J. Appl. Meteor.*, 40, 1665-1682

- 835 • Palm, S. P., D. L. Hlavka, P. Selmer, R. Pauly, 2016: the Cloud Aerosol Transport System  
836 (CATS) Data Product Catalog release 3.0. Retrieved on January 23rd 2018 from  
837 [https://cats.gsfc.nasa.gov/media/docs/CATS\\_Data\\_Products\\_Catalog.pdf](https://cats.gsfc.nasa.gov/media/docs/CATS_Data_Products_Catalog.pdf)
- 838 • Pappalardo, G., Amodeo, A., Apituley, A., Comeron, A., Freudenthaler, V., Linné, H.,  
839 Ansmann, A., Bösenberg, J., D'Amico, G., Mattis, I., Mona, L., Wandinger, U., Amiridis,  
840 V., Alados-Arboledas, L., Nicolae, D., and Wiegner, M.: EARLINET: towards an  
841 advanced sustainable European aerosol lidar network, *Atmos. Meas. Tech.*, 7, 2389-  
842 2409, doi:10.5194/amt-7-2389-2014, 2014
- 843 • Philippon, N. et al. (2016), Analysis of the diurnal cycles for a better understanding of  
844 the mean annual cycle of forests greenness in Central Africa, *Agricultural and Forest  
845 Meteorology*, 223, 81–94, doi:10.1016/j.agrformet.2016.04.005.
- 846 • Protat, A., J. Delanoë, A. Plana-Fattori, P. T. May, and E. J. O'Connor (2009), The  
847 statistical properties of tropical ice clouds generated by the West African and  
848 Australian monsoons, from ground-based radar-lidar observations, *QJRM*, 136(S1),  
849 345–363, doi:10.1002/qj.490.
- 850 • Reverdy, M., Noel, V., Chepfer, H., & Legras, B. (2012). On the origin of subvisible  
851 cirrus clouds in the tropical upper troposphere. *Atmospheric Chemistry and Physics*,  
852 12(24), 12081–12101. <http://doi.org/10.5194/acp-12-12081-2012>
- 853 • Reverdy, M., H. Chepfer, D. Donovan, V. Noel, G. Cesana, C. Hoareau, M. Chiriaco, and  
854 S. Bastin (2015), An EarthCARE/ATLID simulator to evaluate cloud description in  
855 climate models, *J. Geophys. Res.*, 120(2), 11, doi:10.1002/2015JD023919.
- 856 • Rossow, W. B., 1989: Measuring cloud properties from space: A review. *J. Climate*, 2,  
857 201–213
- 858 • Rozendaal, M. A., Leovy, C. B., and Klein, S. A.: An Observational Study of Diurnal  
859 Variations of Marine Stratiform Cloud, *J. Climate*, 8, 1795–1809, 1995.
- 860 • Sassen, K., and S. Benson (2001), A midlatitude Cirrus Cloud Climatology from the  
861 Facility for Atmospheric Remote Sensing. Part II : microphysical properties derived  
862 from lidar depolarisation, *J. Atmos. Sci.*, 58, 2103–2112, doi:10.1175/1520-  
863 0469(2001)058<2103:AMCCCF>2.0.CO;2.



- 864 • Sassen, K., Z. Wang, and D. Liu (2009), Cirrus clouds and deep convection in the  
865 tropics: Insights from CALIPSO and CloudSat, *J. Geophys. Res.*, 114, D00H06,  
866 doi: 10.1029/2009JD011916.
- 867 • Sassen, K., and Z. Wang (2012), The Clouds of the Middle Troposphere: Composition,  
868 Radiative Impact, and Global Distribution, *Surveys in Geophysics*, 33(3-4), 677–691,  
869 doi:10.1007/s10712-011-9163-x.
- 870 • Sèze, G., J. Pelon, M. Derrien, H. Le Gléau, and B. Six (2014), Evaluation against  
871 CALIPSO lidar observations of the multi-geostationary cloud cover and type dataset  
872 assembled in the framework of the Megha-Tropiques mission, *QJRMS*, 141(688),  
873 774–797, doi:10.1002/qj.2392.
- 874 • Shang, H., H. Letu, T. Y. Nakajima, Z. Wang, R. Ma, T. Wang, Y. Lei, D. Ji, S. Li, and J. Shi  
875 (2018), Diurnal cycle and seasonal variation of cloud cover over the Tibetan Plateau  
876 as determined from Himawari-8 new-generation geostationary satellite data,  
877 *Scientific Reports*, 1–8, doi:10.1038/s41598-018-19431-w.
- 878 • Soden, B. J. (2000), The diurnal cycle of convection, clouds, and water vapor in the  
879 tropical upper troposphere. *Geophys. Res. Lett.* 27 (15), 2173-2176. doi:  
880 10.1029/2000GL011436
- 881 • Stephens, G. L., & Kummerow, C. D. (2007). The Remote Sensing of Clouds and  
882 Precipitation from Space: A Review. *Journal of the Atmospheric Sciences*, 64(11),  
883 3742–3765. <http://doi.org/10.1175/2006JAS2375.1>
- 884 • Stephens, G., D. Winker, J. Pelon, C. Trepte, D. Vane, C. Yuhas, T. L’Ecuyer, and M.  
885 Lebsock, 2018: [CloudSat and CALIPSO within the A-Train: Ten Years of Actively](https://doi.org/10.1175/BAMS-D-16-0324.1)  
886 [Observing the Earth System](https://doi.org/10.1175/BAMS-D-16-0324.1). *Bull. Amer. Meteor. Soc.*, 99, 569–  
887 581, <https://doi.org/10.1175/BAMS-D-16-0324.1>
- 888 • Stubenrauch, C.J., A. Chédin, G. Rädcl, N.A. Scott, and S. Serrar, 2006: Cloud  
889 Properties and Their Seasonal and Diurnal Variability from TOVS Path-B. *J. Climate*,  
890 19, 5531–5553, <https://doi.org/10.1175/JCLI3929.1>
- 891 • Taylor, S., Stier, P., White, B., Finkensieper, S., and Stengel, M.: Evaluating the diurnal  
892 cycle in cloud top temperature from SEVIRI, *Atmos. Chem. Phys.*, 17, 7035-7053,

- 893 <https://doi.org/10.5194/acp-17-7035-2017>, 2017
- 894 • Vaughan, M. A., K. A. Powell, D. M. Winker, C. A. Hostetler, R. E. Kuehn, W. H. Hunt, B.  
895 J. Getzewich, S. A. Young, Z. Liu, and M. J. McGill (2009), Fully Automated Detection  
896 of Cloud and Aerosol Layers in the CALIPSO Lidar Measurements, *J. Atmos. Oceanic  
897 Technol.*, 26(10), 2034–2050, doi:10.1175/2009JTECHA1228.1.
- 898 • Wilson, A. M. and Barros, A. P.: Orographic Land–Atmosphere Interactions and the  
899 Diurnal Cycle of Low-Level Clouds and Fog, *J. Hydrometeor.*, 18(5), 1513–1533,  
900 doi:10.1175/JHM-D-16-0186.1, 2017.
- 901 • Winker, D., M. A. Vaughan, A. Omar, Y. Hu, and K. A. Powell (2009), Overview of the  
902 CALIPSO mission and CALIOP data processing algorithms, *J. Atmos. Oceanic Technol.*,  
903 26, 2310–2323.
- 904 • Winker DM, Pelon J, Coakley JA Jr, Ackerman SA, Charlson RJ, Colarco PR, Flamant P,  
905 Fu Q, Hoff RM, Kittaka C, Kubar TL, Le Treut H, McCormick MP, Mé g ie G, Poole L,  
906 Powell K, Trepte C, Vaughan MA, Wielicki BA. 2010. The CALIPSO mission: A global 3D  
907 view of aerosols and clouds. *Bull. Am. Meteorol. Soc.* 91: 1211–1229.
- 908 • Winker, D., Chepfer, H., Noel, V. and X. Cai: Observational Constraints on Cloud  
909 Feedbacks: The Role of Active Satellite Sensors. *Survey in Geophys* (2017).  
910 Doi:10.1007/s10712-017-9452-0
- 911 • Wylie, D. (2008), Diurnal Cycles of Clouds and How They Affect Polar-Orbiting  
912 Satellite Data, *J. Climate*, 21(16), 3989–3996, doi:10.1175/2007JCLI2027.1.
- 913 • Yin, J., & Porporato, A. (2017). Diurnal cloud cycle biases in climate models. *Nature  
914 Communications*, 8(1), 2269.
- 915 • Yorks, J. E., D. L. Hlavka, W. D. Hart, M. J. McGill, 2011: Statistics of Cloud Optical  
916 Properties from Airborne Lidar Measurements. *J. Atmos. Oceanic Technol.*, 28, 869–  
917 883. doi: <http://dx.doi.org/10.1175/2011JTECHA1507.1>
- 918 • Yorks, J. E., M. J. McGill, S. P. Palm, D. L. Hlavka, P. A. Selmer, E. P. Nowottnick, M. A.  
919 Vaughan, S. D. Rodier, and W. D. Hart (2016a), An overview of the CATS level 1  
920 processing algorithms and data products, *Geophys. Res. Lett.*, 43, 4632–4639,  
921 doi:[10.1002/2016GL068006](https://doi.org/10.1002/2016GL068006).

- 922 • Yorks, J. E., S. P. Palm, M. J. McGill, D. L. Hlavka, W. D. Hart, P. A. Selmer, E.  
923 Nowottnick (2016b), CATS Algorithm Theoretical Basis Document, Level 1 and Level 2  
924 Data Products, release 1.2. Retrieved on February 13th 2018 from  
925 [https://cats.gsfc.nasa.gov/media/docs/CATS\\_ATBD.pdf](https://cats.gsfc.nasa.gov/media/docs/CATS_ATBD.pdf)
- 926 • Yorks, J. E., S.D. Rodier, E. Nowottnick, P.A. Selmer, M.J. McGill, S.P. Palm, and M. A.  
927 Vaughan (2018), CATS Level 2 Vertical Feature Mask Algorithms and Data Products:  
928 An Overview and Initial Assessment, Atmos. Meas. Tech. Discuss., in preparation.
- 929 • Zhao, W., R. Marchand, and Q. Fu (2017), The diurnal cycle of clouds and  
930 precipitation at the ARM SGP site: Cloud radar observations and simulations from the  
931 multiscale modeling framework, J. Geophys. Res., 122(14), 7519–7536,  
932 doi:10.1002/2016JD026353.

932 Figures.

933

934 Figure 1: (top) Number of CATS profiles in 2°x2° lon-lat boxes sampled during JJA 2015-2016-  
935 2017, with unsampled latitudes in grey. (bottom) Evolution of the vertical profile of Cloud  
936 Fraction as a function of local time of observation over the Ocean (left) and Land (right),  
937 using CATS detections made in JJA from 2015 to 2017.

938

939 Figure 2. Like Fig. 1, over the North Hemisphere midlatitudes (top row) and Tropics (second  
940 row), the South Hemisphere Tropics (third row) and midlatitudes (bottom row) during JJA  
941 from 2015 to 2017.

942

943 Figure 3: Same as Fig. 2, considering data CATS measured during the boreal winter (DJF,  
944 from 2015 to 2017).

945

946 Figure 4: The diurnal cycle of cloud fraction profiles as seen ground-based instruments (see  
947 text, left column) and the CATS instrument (right column) during JJA 2015-2017 at or in a  
948 10°x10° lat-lon box centered on (first row) SIRTA, considering only sunlit conditions, (second  
949 row) ARM-SGP, (third row) ARM-ENA. Times are local.

950

951 Figure 5: Diurnal cycle of the cloud fraction profiles observed by CATS over different  
952 continents a) NH America, b) Europe, c) China, d) NH Africa, e) SH America, f) SH Africa, g)  
953 Australia, averaged over the summer months (JJA in the North Hemisphere, DJF in the South  
954 Hemisphere) from 2015 to 2017. For each region we considered all profiles sampled over  
955 land within the boundaries shown by the inset map. CF over Europe do not extend to  
956 altitudes as high as the rest, as it is the only region that does not include part of the Tropical  
957 band.

958

959 Figure 6: Mean diurnal variations of low-level (solid line) and high-level (dotted line) cloud  
960 amounts (%) every 3 hours in five zonal bands over ocean (left) and land (right) in JJA from  
961 CATS for the period 2015-2017.

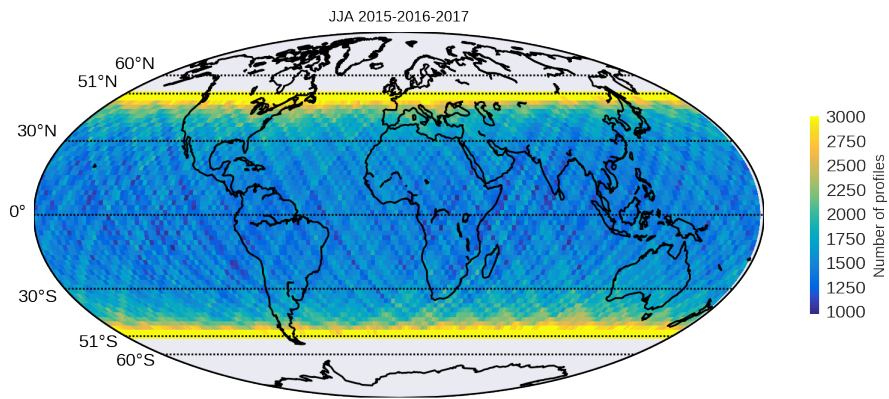
962 Figure 7: Vertical Profiles of Cloud Fraction observed by CALIPSO (full line) and CATS (dashed  
963 line) between  $\pm 51^\circ$  around 0130AM (blue), 0130PM (red) and at all times (black), over ocean  
964 (left) and land (right). Measurements were weighted based on the latitude at which they  
965 were made, to account for the different zonal sampling distributions of both instruments.  
966 CALIOP cloud profiles were built using cloud layers from the CALIPSO v4.10 level 2, 5-km  
967 cloud layer product. Only layers with a Cloud/Aerosol Discrimination score (CAD\_Score)  
968 above 0.7 were considered to build the CALIOP profiles, and layers with a  
969 Feature\_Type\_Score above 5 were considered to build the CATS profiles. For both  
970 instruments, we used JJA observations from 2015 to 2017.

971

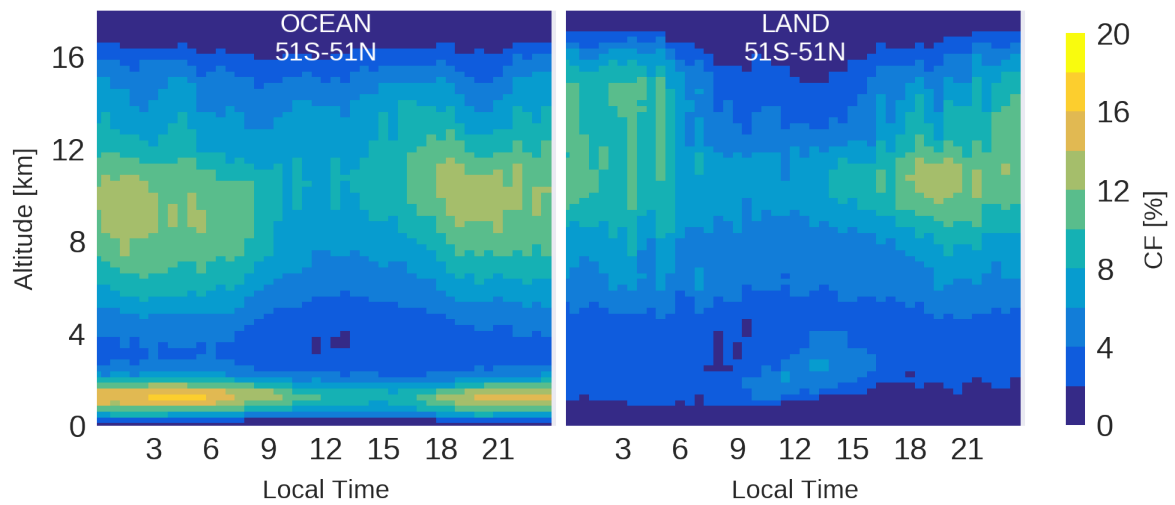
972 Figure 8: Mean Cloud fraction profiles observed by CATS at the overpass local time of the  
973 sun-synchronous space lidars (CALIPSO and the A-train 01:30UTC, ADM 06:00UTC, Earth-  
974 CARE 02:00UTC) compared to the envelope of the whole cloud fraction profile diurnal cycle  
975 observed by CATS (white), averaged between  $\pm 51^\circ$  over ocean (left) and land (right).  
976 CALIPSO and Earth-CARE are dedicated to clouds an aerosols studies, while ADM is primarily  
977 dedicated to wind measurements in non-cloudy conditions. We used CATS observations  
978 during JJA from 2015 to 2017.

979

980

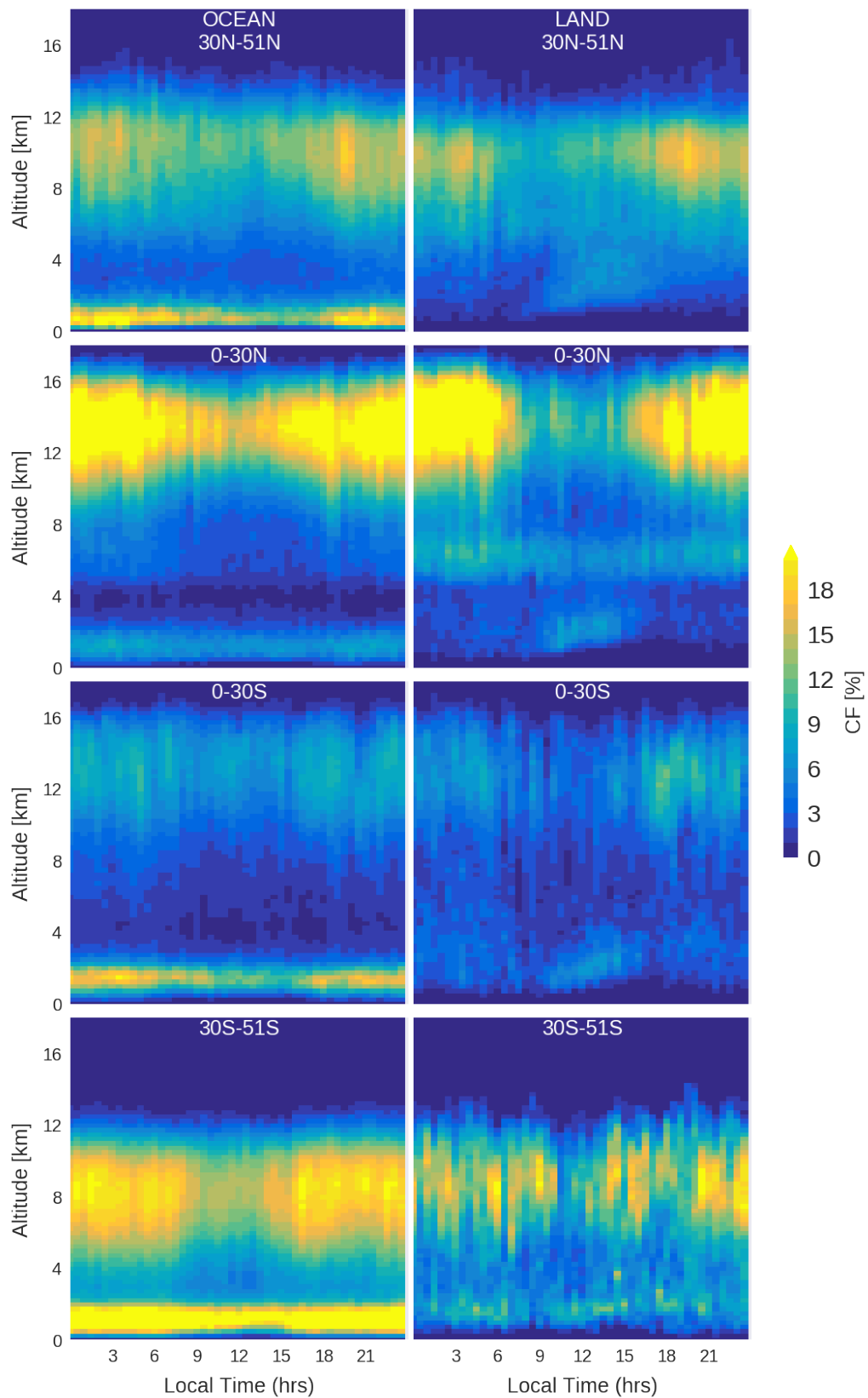


981



982

983 Figure 1: (top) Number of CATS profiles in  $2^\circ \times 2^\circ$  lon-lat boxes sampled during JJA 2015-2016-  
 984 2017, with unsampled latitudes in grey. (bottom) Evolution of the vertical profile of Cloud  
 985 Fraction as a function of local time of observation over the Ocean (left) and Land (right),  
 986 using CATS detections made in JJA from 2015 to 2017.

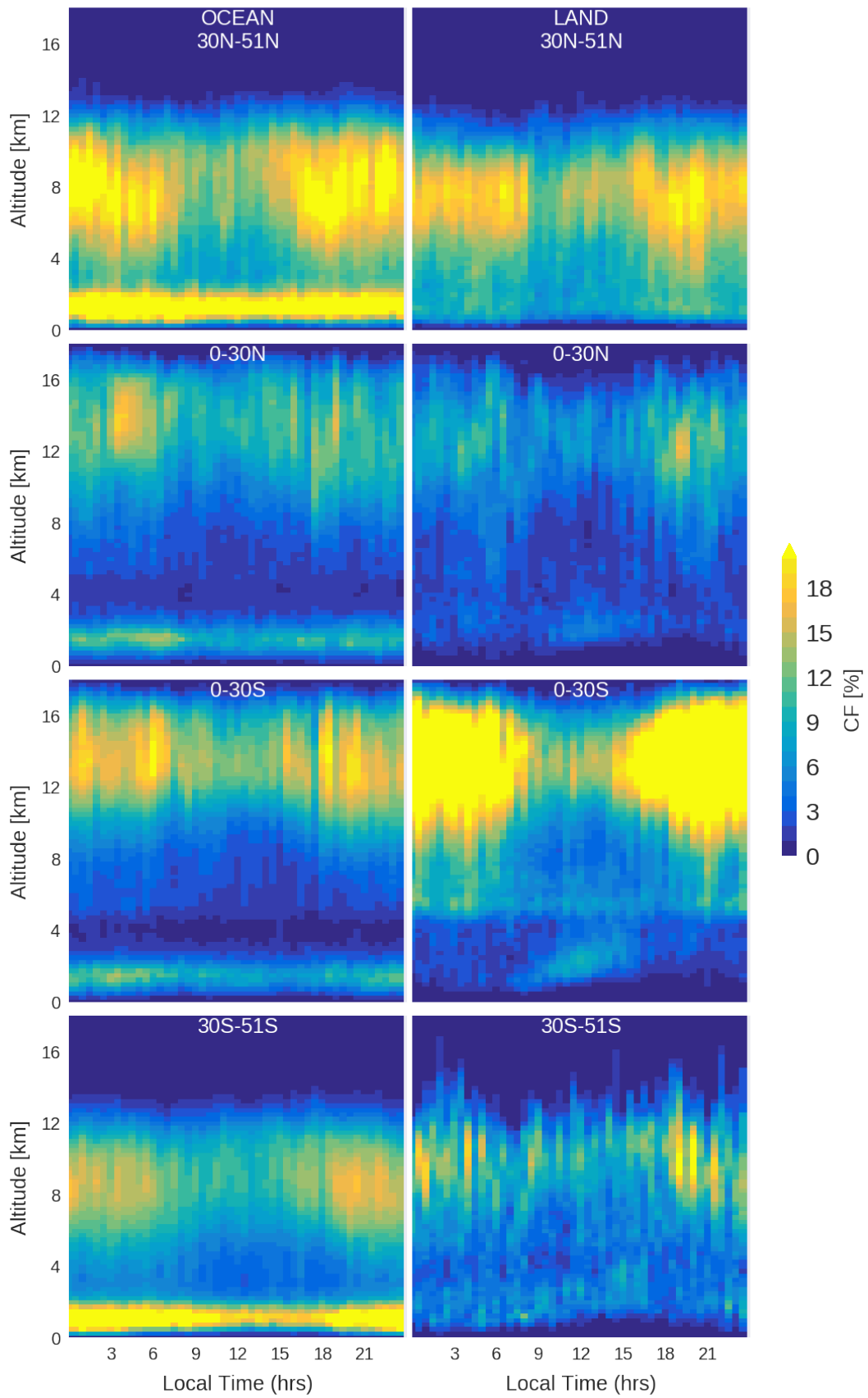


987

988 Figure 2. Like Fig. 1, over the North Hemisphere midlatitudes (top row) and Tropics (second

989 row), the South Hemisphere Tropics (third row) and midlatitudes (bottom row) during JJA

990 from 2015 to 2017.

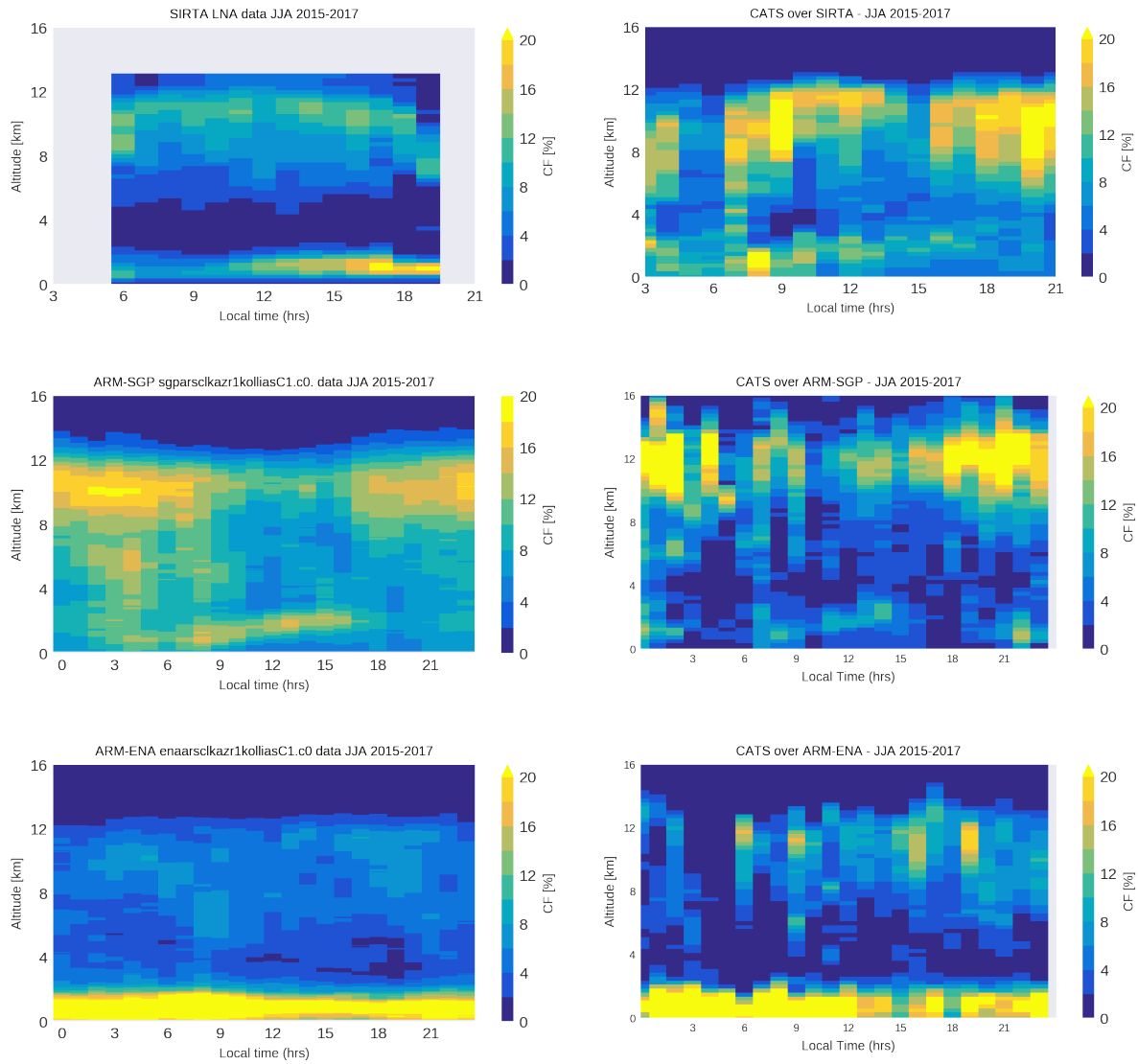


991

992 Figure 3: Same as Fig. 2, considering data CATS measured during the boreal winter (DJF,

993 from 2015 to 2017).

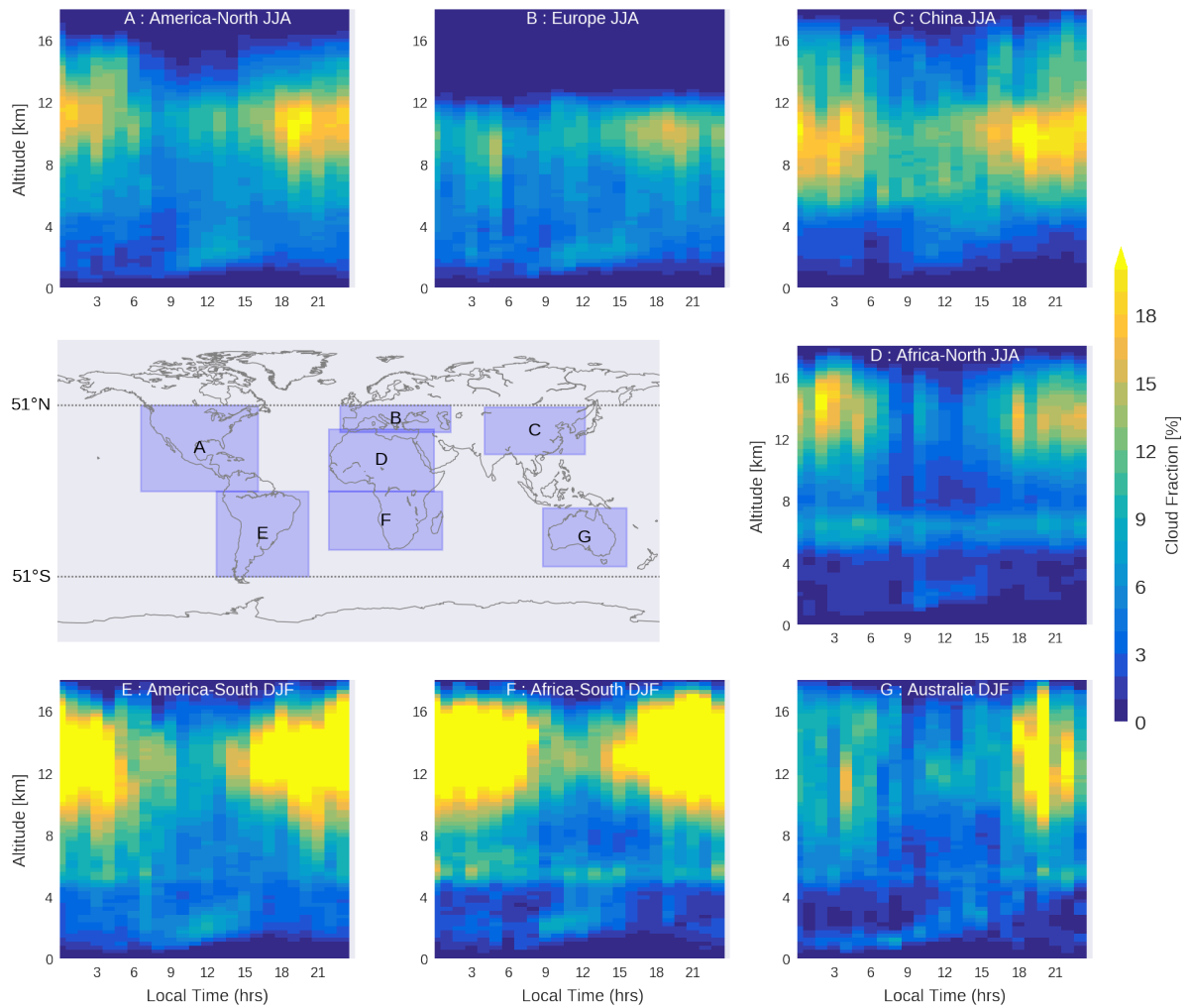




994

995 Figure 4: The diurnal cycle of cloud fraction profiles as seen ground-based instruments (see  
 996 text, left column) and the CATS instrument (right column) during JJA 2015-2017 at or in a  
 997  $10^{\circ} \times 10^{\circ}$  lat-lon box centered on (first row) SIRTA, considering only sunlit conditions, (second  
 998 row) ARM-SGP, (third row) ARM-ENA. Times are local.

999



1000

1001

1002

1003

1004

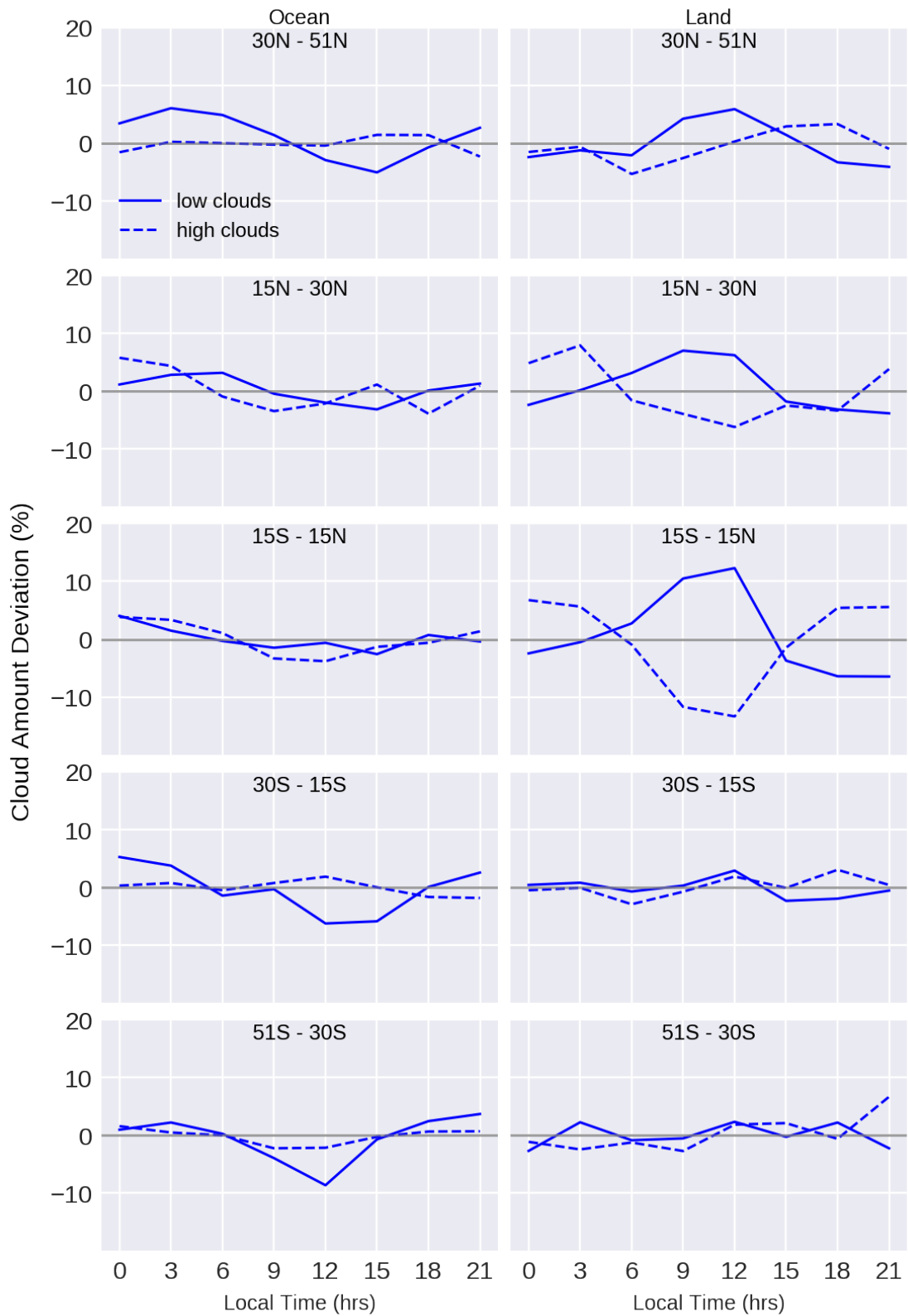
1005

1006

1007

1008

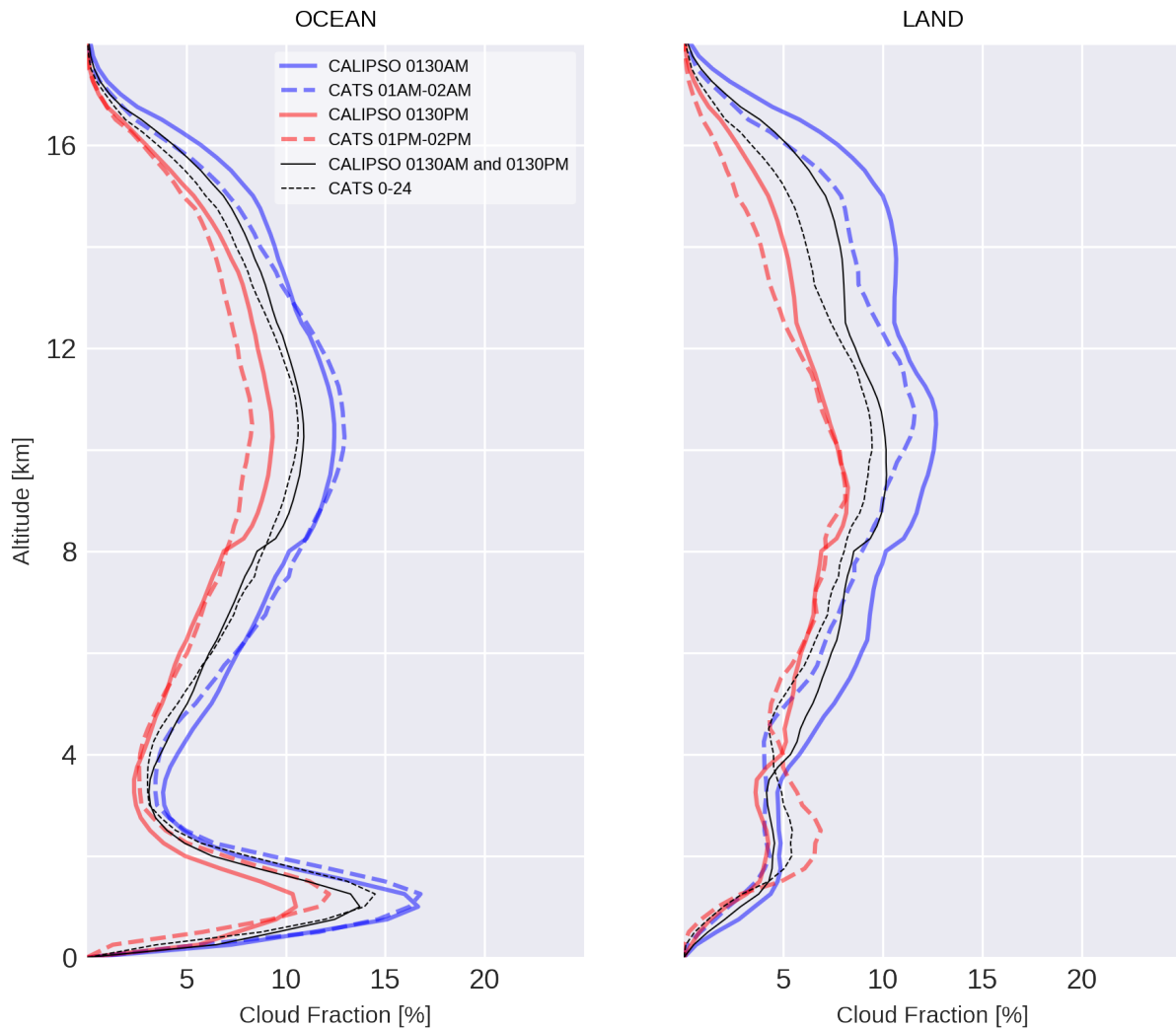
Figure 5: Diurnal cycle of the cloud fraction profiles observed by CATS over different continents A) NH America, B) Europe, C) China, D) NH Africa, E) SH America, F) SH Africa, G) Australia, averaged over the summer months (JJA in the North Hemisphere, DJF in the South Hemisphere) from 2015 to 2017. For each region we considered all profiles sampled over land within the boundaries shown by the inset map. CF over Europe do not extend to altitudes as high as the rest, as it is the only region that does not include part of the Tropical band.



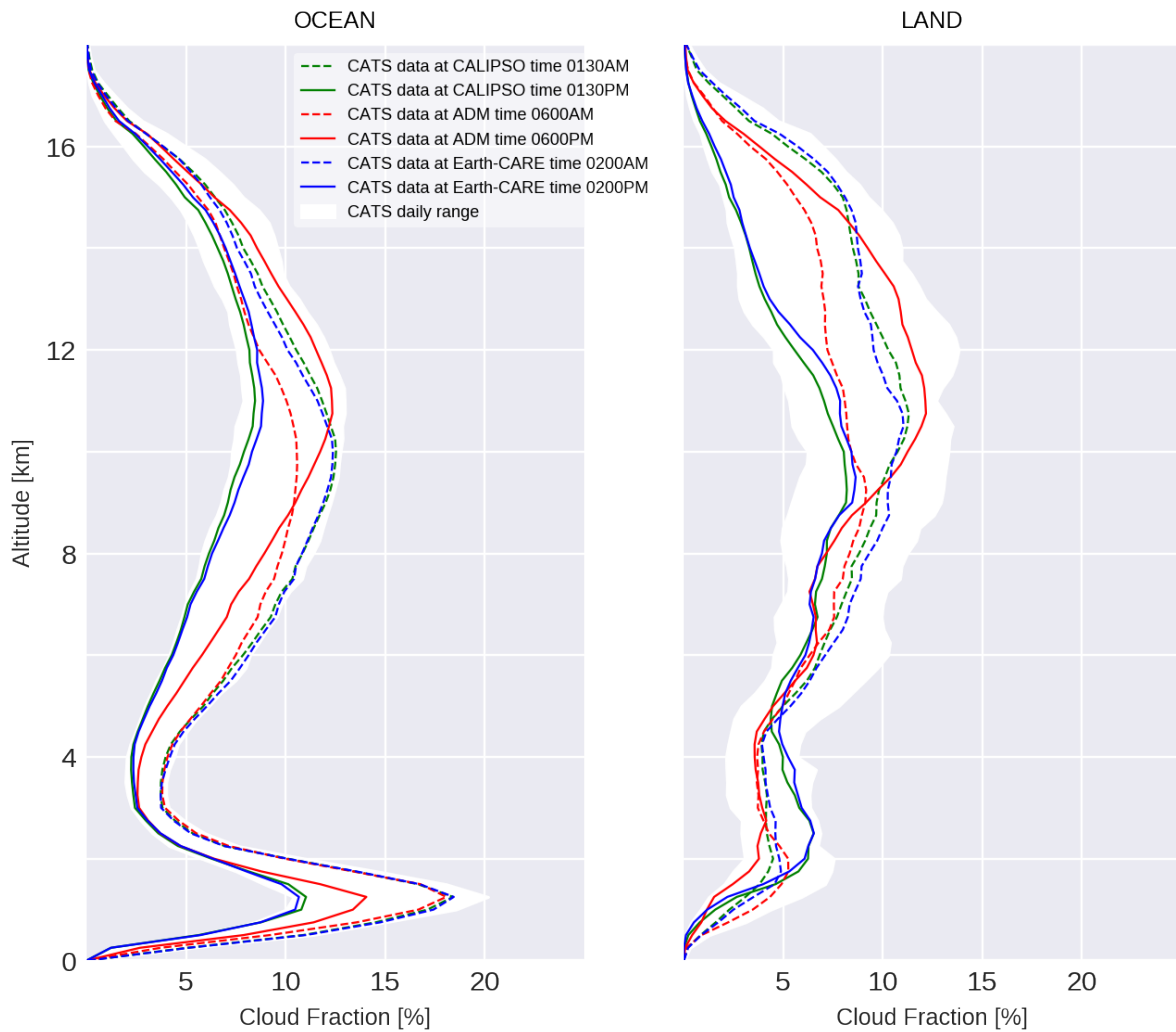
1009

1010 Figure 6: Mean diurnal variations of low-level (solid line) and high-level (dotted line) cloud  
 1011 amounts (%) every 3 hours in five zonal bands over ocean (left) and land (right) in JJA from  
 1012 CATS for the period 2015-2017.

1013



1014  
 1015 Figure 7: Vertical Profiles of Cloud Fraction observed by CALIPSO (full line) and CATS (dashed  
 1016 line) between  $\pm 51^\circ$  around 0130AM (blue), 0130PM (red) and at all times (black), over ocean  
 1017 (left) and land (right). Measurements were weighted based on the latitude at which they  
 1018 were made, to account for the different zonal sampling distributions of both instruments.  
 1019 CALIOP cloud profiles were built using cloud layers from the CALIPSO v4.10 level 2, 5-km  
 1020 cloud layer product. Only layers with a Cloud/Aerosol Discrimination score (CAD\_Score)  
 1021 above 0.7 were considered to build the CALIOP profiles, and layers with a  
 1022 Feature\_Type\_Score above 5 were considered to build the CATS profiles. For both  
 1023 instruments, we used JJA observations from 2015 to 2017.



1024

1025 Figure 8: Mean Cloud fraction profiles observed by CATS at the overpass local time of the  
 1026 sun-synchronous space lidars (CALIPSO and the A-train 01:30UTC, ADM 06:00UTC, Earth-  
 1027 CARE 02:00UTC) compared to the envelope of the whole cloud fraction profile diurnal cycle  
 1028 observed by CATS (white), averaged between  $\pm 51^\circ$  over ocean (left) and land (right).

1029 CALIPSO and Earth-CARE are dedicated to clouds and aerosols studies, while ADM is primarily  
 1030 dedicated to wind measurements in non-cloudy conditions. We used CATS observations  
 1031 during JJA from 2015 to 2017.